batteries

MDPI

Review

Review of Cell Level Battery (Calendar and Cycling) Aging Models: Electric Vehicles

Gulsah Yarimca and Erdal Cetkin *

Department of Mechanical Engineering, Izmir Institute of Technology, İzmir 35430, Turkey; gulsahyarimca@iyte.edu.tr
* Correspondence: erdalcetkin@iyte.edu.tr

Abstract: Electrochemical battery cells have been a focus of attention due to their numerous advantages in distinct applications recently, such as electric vehicles. A limiting factor for adaptation by the industry is related to the aging of batteries over time. Characteristics of battery aging vary depending on many factors such as battery type, electrochemical reactions, and operation conditions. Aging could be considered in two sections according to its type: calendar and cycling. We examine the stress factors affecting these two types of aging in detail under subheadings and review the battery aging literature with a comprehensive approach. This article presents a review of empirical and semi-empirical modeling techniques and aging studies, focusing on the trends observed between different studies and highlighting the limitations and challenges of the various models.

Keywords: electric vehicles; battery aging; battery aging models; calendar aging; cycling; aging

check for updates

Citation: Yarimca, G.; Cetkin, E. Review of Cell Level Battery (Calendar and Cycling) Aging Models: Electric Vehicles. *Batteries* **2024**, *10*, 374. https://doi.org/10.3390/batteries10110374

Academic Editor: George Zheng Chen

Received: 16 August 2024
Revised: 4 October 2024
Accepted: 17 October 2024
Published: 22 October 2024

1. Introduction

The majority (almost 80%) of global energy demand is supplied from fossil fuels [1]. The emissions associated with them is responsible for environmental pollution and climate change. The integration of renewable energy sources into transportation has gained momentum due to the increased use of electric vehicles in recent years. Consequently, the emissions associated with transportation would be notably decreased, contributing to the alleviation of environmental pollution and the mitigation of climate change [2]. Furthermore, some additional benefits of electric vehicles (EVs) in comparison to the conventional internal combustion vehicles are enhanced sustainability, diversification of energy sources, quiet operation (noise pollution), and low operating costs [3,4].

The International Energy Agency reports that many developed nations are transitioning to electric vehicles due to financial and political support, as well as regulations targeting carbon emissions from fossil fuels [5]. Therefore, it is evident that EVs will become widespread in the upcoming decade. Thus, the importance of batteries is becoming essential more than ever. There are many distinct types of batteries used in electric vehicles depending on their chemistry, shape, characteristics, etc. Li-ion (Lithium Ion) batteries are the most preferred ones for EVs instead of NiMH (Nickel Metal Hydride) and Pb-acid (Lead-Acid) batteries [6].

Lithium-ion batteries are the most commonly used battery type in current electric vehicles, thanks to their advanced technological benefits compared to their competitors [7]. Lithium-ion batteries are in demand in automotive and aerospace applications due to many advantages, such as high power, a high charging rate, high capacity, no memory effect, a cost-effective purchase, and low self-discharge [8,9]. While some Li-ion chemistries may have specific thermal or performance limitations, overall charge/discharge efficiency is much higher compared to other electrochemical technologies. Also, while some chemistries have demonstrated limited life cycles, certain commercial EV Li-ion batteries, such as LFP/graphite and NCA/graphite, have already shown the ability to exceed 5000 full cycles at room temperature. There are also distinct chemistries for Li-ion cells, which yield

unique performance, safety, and cost characteristics. Most commercial Li-ion cells use intercalating compounds as active materials. The negative electrode (negative electrode) is usually graphite, and there are five distinct types of lithium-ion batteries named after their positive electrode (positive electrode) materials: Lithium Cobalt Oxide (LCO), Lithium Iron Phosphate (LFP), Lithium Manganese Oxide (LMO), Lithium Nickel Manganese Cobalt Oxide (NMC), and Lithium Nickel Cobalt Aluminum Oxide (NCA). Some manufacturers dope LMO with small amounts of Nickel (Ni), Aluminum (Al), or other materials to enhance its energy density and thermal stability, making it more suitable for high-performance applications in electric vehicles. In addition, if the negative electrode material of a Li-ion battery is Lithium Titanium Oxide (LTO) instead of graphite, the battery is named after the negative electrode material used [10]. While mobile electronic devices have traditionally been powered by high-energy-density lithium batteries with LCO ($LiCoO_2$) positive electrodes and graphite negative electrodes, in recent years, NCA and NMC lithium batteries have become more common due to their lower costs. LFP ($LiFePO_4$), NCA, NMC, and LTO are widely used in EVs due to their high energy density compared to other chemistries, whereas LMO is no longer commonly used in EV applications due to its poor calendar life and lower energy density [11,12].

Battery cell performance and useful capacity degrades over time, while internal resistance increases due to the aging of batteries [13–16]. Batteries in EVs and hybrid electric vehicles (HEVs) are generally considered to reach end-of-life (EOL) when their state-of-health (SoH) drops to 80% of the original capacity, as defined by most international standards, and should be replaced. In addition, factors such as battery resistance, power performance, and warranty considerations influence battery replacement decisions. Therefore, critical measures should be taken to design battery packs for HEVs/EVs [17,18].

Aging is caused by various chemical mechanisms that affect the electrolyte, electrodes, separator, current collectors, and separator (Figure 1 [19,20]). The predominant cause of capacity loss, as acknowledged by many authors, is attributed to the loss of lithium inventory [21–23]. The degradation mechanisms of the negative electrode and positive electrode differ significantly. In the negative electrode, lithium inventory loss primarily occurs due to the formation of an insulating solid electrolyte interphase (SEI) at the negative electrode's surface, resulting from the reduction in the electrolyte. This reduction leads to lithium plating and a reduction in available active lithium. In contrast, positive electrode degradation follows a different pathway and contributes less to lithium loss.

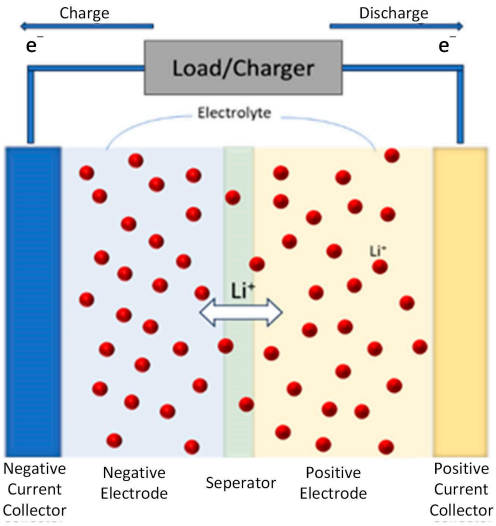

Figure 1. Schematic of lithium-ion battery chemistry.

Consequently, the key factor in limiting capacity is the loss of lithium inventory at the negative electrode [24]. At elevated temperatures and high states of charge (SoC), the SEI layer may form more rapidly. This formation can expose fresh negative electrode material

to the electrolyte, leading to increased reactions between the negative electrode and the electrolyte. As a result, unwanted byproducts may be generated, and the resistance at the negative electrode–electrolyte interface may increase, which is referred to as negative electrode impedance [25,26]. In addition to the effect of SEI growth on the aging of negative electrodes, lithium plating and binder decomposition play an integral role. The aging mechanism in the positive electrode is dominated by active material degradation, mechanical breakage, and electrode separation, where active material detaches from the electrode structure. Electrode separation often occurs due to mechanical stress or degradation of binder materials, leading to reduced battery performance [13]. Figure 2 documents the factors affecting aging, the chemical and physical mechanisms of aging, and their associated degradation modes [27]. This figure provides an insight into the cause–effect relationship and the battery aging event cycle.

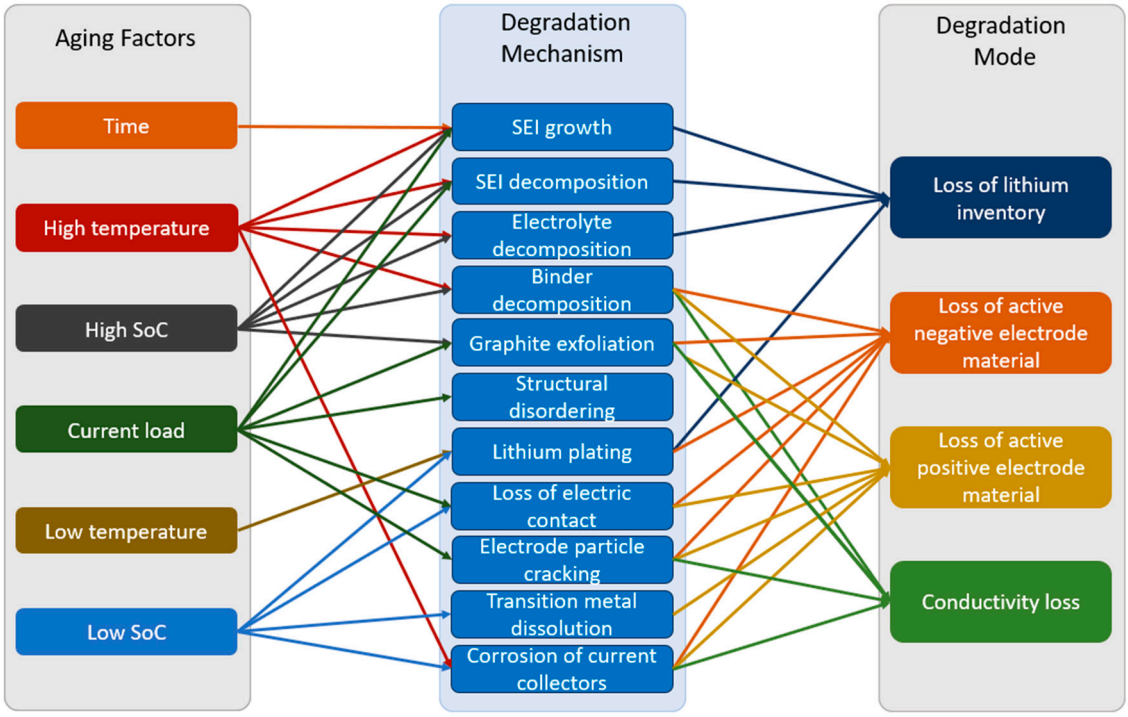

Figure 2. Factors affecting aging, chemical and physical mechanisms, and the effects they cause.

Battery aging can be classified in two major categories: cycling and calendar aging. Calendar aging occurs when the battery is at rest (i.e., lack of charge/discharge cycle), and cycling aging occurs when the battery is experiencing charging/discharging cycles. However, all the cells experiencing charge/discharge cycles also age due to calendric effects, which requires both effects of cycling and calendar aging to be combined to offer a more realistic approach. Battery aging is a complex process as many factors interact with each other, while both environmental conditions and user characteristics (drive cycle profile) play a role on aging. Establishing appropriate aging predictions is essential to ensure the efficient use of battery cells as well their safe operation [20]. SoH depends on charge output, time and operation parameters such as the SoC, temperature, current amplitude, and depth of discharge (DoD) [28–31].

While many external factors affect aging, the most dominant is temperature (generally accepted as more than 30 °C) as it triggers some chemical reactions and accelerates the reaction speed of others on degradation. Likewise, excessive current accelerates aging, which also increases the probability of failure during a cycle [32].

Battery Aging Modeling

There are various methods of predicting lithium-ion battery degradation, which depend on the performance trait being observed (such as capacity degradation or increased resistance), the kind of battery life being evaluated (whether it is based on cycles or calendar), and the overall modeling method. Some of these techniques employ electrochemical models that rely on theory to comprehend and predict the actual reactions that cause degradation within the battery. Other approaches utilize a more empirical method to model battery aging and establish connections between battery aging and specific variables by utilizing experimental data.

Electrochemical models aim to quantify the impact of various factors (T, current, SoC, etc.) of battery aging, and these models are used to optimize the physical aspects of batteries and characterize parameters such as voltage, power, and current. The aim of these approaches is to gain a clear understanding of the specific chemical and physical phenomena that occur during battery usage [7]. Electrochemical models rely on the Butler–Volmer equations and porous electrode theory as well as the single-particle model (SPM) to estimate the performance of a battery [33,34].

Models based on electrical principles use equivalent circuit components (ECMs) to forecast how batteries will behave in terms of their terminal characteristics, such as voltage and current. However, the definition of equivalent circuit varies between studies, and the parameters used to predict battery aging may include both internal battery parameters and resistor aging parameters. By extrapolating degradation trends, predictions can be made about which battery components, like electrolyte, negative electrode, positive electrode, etc., are degrading and at what rate [35,36]. These methods require a diverse and large dataset, and testing is time-consuming.

There are different mathematical models in the literature for predicting battery calendar aging, based on empirical evidence. These models can be divided into two categories: empirical and semi-empirical. The semi-empirical approach aims to combine the advantages of both approaches by using theoretical principles and experimental results to assign values to the fit parameters of the model. Semi-empirical models use a combination of theory and curve fitting [37]. For instance, a theory predicts a linear relationship, and the best linear relationship is found from the available data, even if the best fit curve is non-linear. Semi-empirical cell aging models use limited data from cycled and stored cells under accelerated aging conditions.

Electrochemical approaches are often too complex to be practical, while empirical approaches require a large amount of data and only work under specific experimental conditions. Compared to electrochemical models, semi-empirical models are simpler yet can be applied to a wider range of conditions than empirical models [38,39].

Over the past few years, the emergence of machine learning techniques has brought about significant changes in several fields, particularly in battery aging modeling. Machine learning approaches have shown great potential in predicting battery capacity degradation by analyzing large volumes of data and identifying patterns and trends [40]. These models can account for a wide range of factors that affect battery performance, such as temperature, voltage, and current, and can provide more accurate predictions than traditional models [41]. Due to its easy application and independence from detailed knowledge of degradation mechanisms, machine learning-based methods are widely investigated for promoting empirical state-of-health (SoH) estimation [42]. Li et al. [43] provided an overview of various machine learning algorithms for SoH estimation, which includes Gaussian process regression (GPR), neural networks (NNs), relevance vector machines (RVMs), autoregressive models (AMs), and support vector machines (SVMs), based on real-world data. On the other hand, Ng et al. [44] conducted a comparative analysis between ECMs and physics-based models, where they present a comprehensive survey of the application of machine learning techniques for battery state prediction. Gasper et al. [45] presented a novel approach for identifying empirical models from large sets of algorithmically generated equations by means of two-level optimization and symbolic regression, with a focus

on assessing the reliability of these models. Besides these studies, the existing literature on machine learning algorithms is not comprehensive enough, and their efficiency and application potential are still not fully discussed.

The majority of theoretical models that predict battery aging are based on physical relations. Therefore, experimental and numerical aging studies on battery cells are documented simultaneously to uncover the aging mechanisms and capacity degradation of EV batteries. The literature on semi-empirical aging models is scattered, requiring researchers to invest considerable time and effort in locating and synthesizing relevant studies. This scatter can hinder the efficient advancement of knowledge in the field. To address this gap, our goal was to produce a comprehensive review that systematically organizes and consolidates the scattered information. By bringing together key findings and insights from various sources, we aim to provide a structured and accessible resource that not only facilitates a clearer understanding of semi-empirical aging models but also supports and accelerates future research efforts in this area. This review summarizes the capacity degradation of batteries in EVs, factors affecting battery life, and experimental/semi-empirical prediction models for calendar and cyclic aging. In Section 2, experimental studies for calendar aging are evaluated. Section 2 starts with an overview of relevant aging mechanisms and stress factors for commonly used battery types in calendar aging studies. Then, the studies are analyzed to draw a general inference, and degradation models are examined in detail. In Section 3, experimental studies on cycling aging are examined. The same procedures as those mentioned in Section 2 for calendar aging are also applied to cycling aging under this section.

2. Calendar Aging

Calendar aging includes all aging mechanisms that are in the resting state of battery cells, i.e., absent of charge and discharge cycle [46]. Over time, the chemical reactions occurring within the battery cells during storage gradually degrade the active materials on the electrodes and the electrolyte, leading to capacity degradation. These reactions can lead to the formation of an SEI layer, positive electrode electrolyte interphase (CEI) formation electrolyte decomposition, and changes in electrode materials over time, such as the loss of active material, structural damage, and chemical alterations.

Several interconnected factors contribute to calendar aging in EV batteries. Calendar aging is greatly affected from the SoC, temperature, and the time elapsed [47]. Temperature plays a critical role in calendar aging. Conversely, extremely low temperatures can also impair battery efficiency and performance [48,49]. Manufacturers and battery management systems incorporate temperature control mechanisms to maintain batteries within optimal operating ranges, typically between 25 °C and 30 °C [50,51]. The SoC is another crucial factor affecting calendar aging; storing batteries at high SoC levels for extended periods can increase aging.

This section aims to explore various experimental studies in the literature that have produced noteworthy findings about battery calendar aging. Our primary focus is on highlighting the influence of temperature and the SoC to gain a better understanding of their impact on battery longevity. The ultimate objective of this evaluation is to derive valuable insights that can enhance the lifespan of batteries, leading to improved performance and efficiency.

Wang et al. [39] tested NMC + LMO cells with a 1.5 Ah capacity over 400 days at various temperatures and DoDs. They found that capacity degradation was largely influenced by a loss of lithium inventory, with the highest reduction occurring at 46 °C, resulting in a 22% capacity degradation. They developed a time-dependent model using the Arrhenius correlation to understand temperature's impact, but the model tended to overestimate capacity degradation at higher temperatures of 34 °C and 46 °C compared to the observed results. In another study examining the impact of loss of lithium inventory on capacity degradation at elevated temperatures, Sarasketa-Zabala et al. [52] conducted aging tests on 2.3 Ah LFP cells for 300 to 650 days within a temperature range of 30 °C

to 50 °C. Furthermore, results showed that prolonged storage and temperatures over 40 °C accelerated aging, through active material loss (LAM). They created a model using a combination of storage temperature and SoC parameters based on the Arrhenius law.

Ecker et al. [28] examined the aging of lithium-ion batteries by combining the electric–thermal model with a semi-empirical aging model. They conducted accelerated tests on six Ah NMC batteries over 60 weeks, varying temperature, and the SoC. Cells stored at 65 °C showed gassing processes and rapid failure. Capacity degradation was found to have an exponential relationship with both voltage and temperature, as per their results. Omar et al. [53] conducted calendar life experiments on LFP pouch battery cells with a 7 Ah capacity, testing at four temperatures and three SoCs for 28–280 days. They found that high storage temperatures significantly reduced battery life, with temperature having a greater impact on aging than SoC. Optimal storage conditions were around 25 °C. Aging increased by 120% at 20 °C, 135% at 40 °C, and 138% at 60 °C. In another study that provides evidence supporting the notion that temperature exerts a more significant influence on aging than the SoC, Grolleau et al. [54] studied commercial LFP cells with a 15 Ah capacity, stored at three SoCs and temperatures for 450 days and developed an aging model. Their model accurately predicted degradation based on storage conditions, indicating that capacity degradation depended solely on storage conditions, not aging history.

Kassem et al. [55] investigated the aging of 8 Ah LFP cells for up to 8 months. They found that capacity degradation correlated directly with storage temperature, with severe aging observed at 60 °C. Cyclic lithium loss, attributed to side reactions at the negative electrode, was identified as the primary cause of capacity degradation. Cells aged at higher temperatures exhibited both reversible and irreversible capacity degradations, with irreversible losses being more significant at 60 °C. Werner et al. [38] studied the calendar aging of an NCA cell over 21 months, finding that high temperatures and high SoC levels led to significant self-discharge, particularly at 100% SoC and 60 °C. An empirical model was developed to describe cell degradation, revealing no dependency on temperature path. Similarly, Wildfeuer et al. [56] investigated the aging of 196 lithium-ion cells with 2.5 Ah NCA positive electrodes over 697 days. They discovered that battery lifetimes were underestimated due to inconsistent periodic check procedures and that inspection frequency impacted degradation rates. The effect of the SoC on calendar aging was highest at around an 85% SoC, possibly due to a positive electrode-driven shuttle mechanism.

In another study using the same experimental data, Karger et al. [57] introduced a novel mechanical calendar aging model based on component health states instead of capacity. Utilizing experimental data covering 672 days under diverse temperature and SoC conditions, unlike traditional capacity-based models, this approach focuses on degradation modes and compensates for check-up measurement impacts. It effectively captures dependencies on temperature and the state of charge for the loss of lithium inventory and active positive electrode material, predicting capacity with less than 1% mean deviation for seven storage conditions. Additionally, check-up compensation extends the predicted lifetime by over 150% under certain conditions.

Similar to the impact of elevated temperatures, lower temperatures also exert adverse effects on battery capacity and internal resistance. Additionally, it is important to acknowledge that the influences of low and high temperatures on battery performance can exhibit variations. Jaguemont et al. [58] presented the results of aging tests conducted on a 100 Ah prismatic LFP battery cell under low-temperature conditions. Three cells underwent a standardized driving cycle at −20 °C; 0 °C; and 25 °C while another underwent a calendar test at −20 °C with an SoC maintained at 50% for 400 days. They found that at −20 °C, the battery reached the end-of-life criterion defined as 80% of nominal capacity after 17 days of storage, highlighting the significant impact of cold temperatures on battery lifespan.

Maures et al. [59] introduced a calendar aging model for 2.5 Ah NCA Lithium-ion batteries focusing on time and temperature effects. Their study spanned temperatures from −20 °C to 55 °C at a 95% SoC for 200–300 days. They quantified degradation processes like conductivity loss (CL), LAM, and loss of lithium inventory, modeling them with an

equation based on the Arrhenius law. They found that while LAM and LLI aging followed Arrhenius's law, at lower temperatures, lithium plating became more significant.

Schmalstieg et al. [60] introduced a comprehensive aging model for 2.05 Ah NMC batteries derived from accelerated aging tests. They found that an SoC at 50% had the least impact on calendar aging. After using an electric–thermal model to generate battery SoC and voltage, they proposed a semi-empirical model based on the Arrhenius law to predict battery future calendar aging, revealing that aging speed increased linearly with voltage during calendar aging tests. Hoog et al. [61] proposed a semi-empirical combined lifetime model for 20 Ah NMC cells. Their numerical model predicted a combined lifespan with less than 5% accuracy relative to the experimental results. Unlike other studies, an initial increase in capacity was observed when cells were stored at a low charge state, attributed to electrochemical grinding. This observation indicated that side reactions did not impact SEI growth.

Zheng et al. [62] conducted a comprehensive investigation into the degradation characteristics of high-power 1.06 Ah LFP batteries exposed to various temperatures and SoC levels for 10 months. Under high SoC conditions, they observed significant lithium-ion loss at the LFP positive electrode, along with a minor reduction in capacity at the graphite negative electrode. Also, for LFP cells, Redondo-Iglesias et al. [63] proposed the use of the Eyring acceleration model for calendar aging modeling, which extends Arrhenius's law to other stress constraints. This model, which is not common, was proposed to express the aging laws of batteries in some recent studies [64,65]. Cells may experience self-discharge (SoC shift) during idle operation.

Su et al. [66] investigated the aging of 3 Ah NMC batteries under static and non-static conditions, exploring pathway dependence. During the non-static storage tests, both temperature and SoC changed over time throughout the testing procedure. Results showed consistent cell aging modes across temperatures, with notable acceleration at a 95% state of charge. They developed an empirical model to describe cell aging in static storage tests.

Naumann et al. [67] presented a comprehensive calendar aging study on 2.3 Ah LFP batteries, in which they observed that capacity degradation increased with high storage SoC cells but remained relatively constant in the middle SoC range. They developed a semi-empirical aging model for capacity degradation applicable to all static and dynamic conditions, with model errors below 2.2% for dynamic validation tests. Xu et al. [68] studied the effects of irregular battery operation on battery degradation using LMO cells. The study considered several fundamental theories of battery degradation, including SEI film formation and the Arrhenius law relation. They found that the effect of SoC on capacity degradation becomes more pronounced as storage time increases, i.e., especially after the 2nd year.

Montaru et al. [69] studied capacity degradation in high-temperature, high-SoC conditions, introducing a dual tank aging model. This model combines a physics-based model for SEI growth and an empirical model for electrode capacity degradation [70,71]. The study tested LMO + NMC Li-ion cells, and significant capacity degradation at higher SoC levels and temperatures was attributed to SEI thickness growth. The model demonstrates the evolution of lithium contents, electrode potentials, and electrode capacities.

Calendar aging analysis involves a recurring process of calendar aging and cell characterization. Historically, the impact of cell characterization on the outcomes of calendar aging studies has been generally considered insignificant. Krupp et al. [46] studied calendar aging of 64 Ah NMC cells with periodic characterization measurements. As a result of characterization measurements, they found increased capacity due to improved cell kinetics, resulting in delayed end-discharge voltage and extended capacity. Reduced cell resistance was observed, attributed to increased positive electrode surface area from structural degradation. The study recommends capacity measurements at a current rate of less than 1 C for consistent results. In addition, the observed aging behaviors displayed some deviations from previous studies, notably in the relationship between SoC and capacity loss. Rather

than a linear dependence, a constant capacity loss was identified between 70% and 90% SoC, which was attributed to the influence of cathodic and combined side reactions.

Keil et al. [72] documented calendar aging of three 18,650 lithium-ion cells with distinct positive electrode materials (NCA, NMC, LFP). They showed that there is no linear relation between calendar aging and SoC. In addition, the negative electrode potential has a significant effect on capacity degradation. Capacity degradation during storage is significantly affected by the intermediate negative electrode potential, which typically occurs between a 30% and 60% SoC for NMC and NCA cells and between a 40% and 70% SoC for LFP cells. When SoC values are below 30–40%, the capacity degrades while the negative electrode potential increases. Eddahech et al. [47] explored calendar aging effects on four Li-ion battery chemistries (LMO + NMC, NMC, LFP and NCA) under various temperatures and SoC levels. They found manganese-containing batteries, particularly LMO and NMC, to be sensitive to elevated temperatures, while LFP batteries demonstrated extended calendar life and thermal stability. NCA cells showed a balance between extended life cycles and high-performance efficiency. Geisbauer et al. [73] investigated six li-ion battery chemistries (NCA, NMC, LFP, LCO, LMO, and LTO) under different temperatures and SoC levels for calendar aging. They found that capacity loss was most severe at 60 °C and higher storage voltages, even for titanate oxide cells. NMC, NCA, and LTO cells exhibited the most severe capacity degradation at 60 °C, with NMC and NCA cells showing no open-circuit voltage at the highest storage voltage and 60 °C due to triggered current interruption mechanisms.

2.1. Evaluation of Empirical Calendar Aging Studies

As detailed in Section 2, various experimental studies in the literature explored the impact of aging parameters on calendar aging behavior. Some studies focus solely on time and temperature, while others propose correlations for aging behavior that consider time, SoC, and temperature. A summary of the studies analyzed in this review is presented in Table 1.

The calendar aging factors in lithium-ion batteries contribute to the degradation of the battery through mechanisms such as the loss of lithium inventory, the loss of active material in the electrodes, and the decline in electrical conductivity [39,59]. Specifically, the loss of lithium inventory occurs due to side reactions that consume Li-ions, such as the formation of SEI on the surface of graphite negative electrodes, electrolyte degradation processes, and binder dissociation. These side reactions trap Li-ions in inactive forms, such as lithium plating or SEI formation, preventing them from participating in further reactions and leading to gradual capacity degradation. SEI growth is particularly affected by the SoC, temperature, and storage time. As the SEI layer thickens, some active materials such as the negative electrode material become less electrochemically active, resulting in negative electrode active material loss, which accelerates calendar aging [52,69]. Electrolyte decomposition in lithium-ion batteries can trigger chemical reactions that corrode electrodes, form insulating layers, and cause structural damage. Decomposition of the electrolyte and irreversible phase transition effects lead to the loss of active material during calendar aging. The loss of electrical conductivity is related to the deterioration of the collectors and connectors. Lithium inventory loss and active material loss are the dominant modes of calendar aging [18].

The degradation of batteries may exhibit varying chemical reactions at high and low temperatures. High temperatures over 40 °C can cause lithium loss, resulting in less available lithium for intercalation and inducing capacity degradation [14,74]. High temperatures can lead to increased chemical activity, causing the breakdown of active materials and the formation of unwanted compounds. This phenomenon ultimately results in a reduction in the battery's capacity and performance, which means that an EV's range on a single charge will diminish more rapidly in hotter climates [28,38,39,47,52–55].

Table 1. Overview of calendar aging studies for EVs reported in the literature, with study conditions and experimental data.

Study	Chemistry	Capacity (Ah)	Storage Time (Days)	Parameters	
				Temp. (°C)	SoC (%)
Eddahech et al. [47]	NMC, LMO, NCA and LFP	5.3, 5.3, 12 and 8 respectively	1000–1200	45 and 60	65 and 100
Geisbauer et al. [73]	NCA, NMC, LFP, LCO, LMO, and LTO	1.3 to 2.6	120–150	18.5, 50, and 60	2, 38, and 100
Keil et al. [72]	NCA, NMC, and LFP	2.8, 2.05 and 1.1, respectively	270–300	25, 40, and 50	0 to 100
Wang et al. [39]	NMC + LMO	1.5	400–600	10, 20, 34, and 46	50
Montoru et al. [69]	NMC + LMO	43	380–700	0, 25, 45, and 60	0, 30, 65, 80, and 100
Sarsketa-Zabala et al. [52]	LFP	2.3	300–650	30, 40, and 50	30, 60, and 90
Omar et al. [53]	LFP	7.	28,280	10, 25, 40, and 60	25, 50, and 100
Grolleau et al. [54]	LFP	15	420–480	30, 45, and 60	30, 65, and 100
Kassem et al. [55]	LFP	8	230	30, 45, and 60	30, 65, and 100
Zheng et al. [62]	LFP	1.06	280	25, 40, and 55	50, 60, and 100
Redondo-Iglesias et al. [63]	LFP	2.3	500–800	30, 45, and 60	30, 65, and 100
Jaguemont et al. [58]	LFP	100	400	−20	50
Naumann et al. [67]	LFP	2.3	810	0, 25, 40, and 60	0 to 100
Ecker et al. [28]	NMC	6	420	25, 35, 50, and 65	20, 50, 80, and 100
Schmalstieg et al. [60]	NMC	2.05	330–520	35, 40, and 50	0, 10, 20, 30, 50, 60, 70, 80, 85, 90, and 95
Su et al. [66]	NMC	3	240	45, 53, and 60	40, 60, 80, and 95
Hoog et al. [61]	NMC	20	470	25, 35, and 45	20 to 80
Krupp et al. [46]	NMC	64	450	23 and 40	50, 70, and 90
Werner et al. [38]	NCA	3.2	590	40, 50, and 60	20, 35, 50, 65, 80, 90, and 100
Wildfeuer et al. [56]	NCA	2.5	697	20, 35, 50, and 60	10, 50, 70, and 100
Maures et al. [59]	NCA	2.5	200–300	−20, 25, and 55	95
Xu et al. [68]	LMO	1.1	1800–3600	15, 25, 35, 45, and 55	60, 80, and 100

High temperatures harm cell lifespan universally, though certain chemistries may be more temperature-sensitive than others. For instance, the NMC + LMO mixture shows a significant increase in degradation rates at temperatures between 40 °C and 60 °C, particularly at a high SoC [39,69]. In contrast, NCA chemistry experiences only a minor change in degradation rates across the same temperature range [38]. The effect of temperature on LMO chemistry is similar to that of the NMC + LMO mixture, but pure LMO cells showed less aging effects compared to the blended NMC + LMO cells [47,72]. On the other hand, cells containing NMC, on their own, have poor high-temperature performance and are susceptible to rapid degradation. High temperatures have a larger impact on aging in LCO cells, followed by NMC, NCA, LMO cells, and to a lesser extent, LFP and LTO cells [28,60,73].

Based on research studies in the literature mentioned earlier, Figure 3 displays experimental measurements of the 200-day capacity degradation of different li-ion battery chemicals under varying storage conditions of 25 °C and 60 °C temperatures [38,46,54,61,66,68,69,73,75]. This graph specifically represents the performance of the batteries discussed in the referenced studies. While there are numerous variations in battery chemistries, the graph is intended to provide an example overview and offer insight into the comparative characteristics of these chemistries. Figure 3 clearly shows that various Li-ion chemistries deteriorate at different rates due to calendar aging. Extreme conditions, such as a 100% SoC and higher temperatures (60 °C), lead to higher capacity loss and increased internal resistance in most cases. Generally, calendar aging has more severe effects on Li-ions stored at 60 °C than those stored at 25 °C.

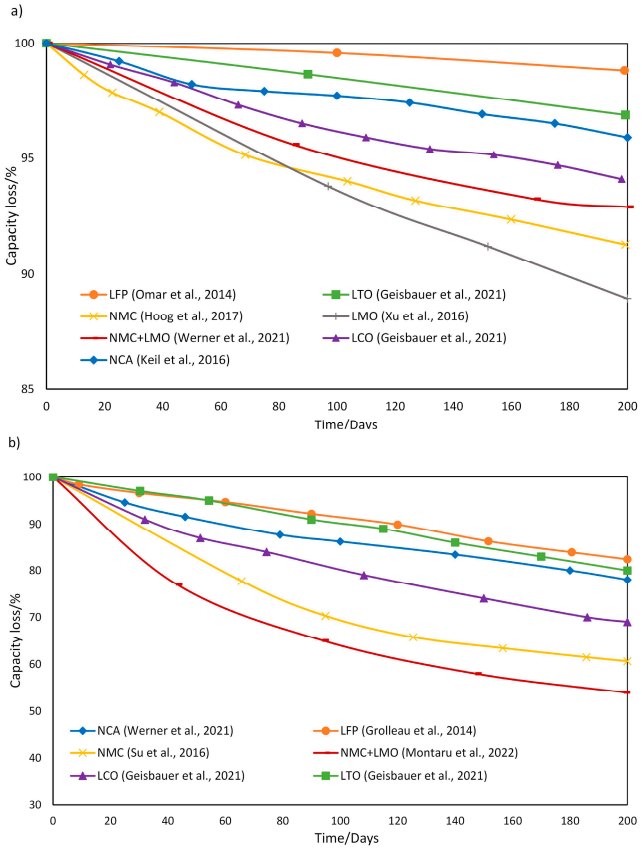

Figure 3. Capacity degradation of seven chemistries over 200 days at storage temperatures (**a**) 25 °C, (**b**) 60 °C, and at 100% SoC conditions in studies in the literature, Refs. [38,46,54,61,66,68,69,73,75].

Battery lifetime also decreases at low temperatures similar to high temperatures where significant deterioration in battery structure observed in both cases [14]. Decreased cycle life due to ambient conditions is one of the major issues that has prevented the widespread adoption of electric vehicles in cold climate regions. Low temperatures can cause a loss of active material, and the ability of the active material within the battery to participate in chemical reactions and facilitate the movement of ions (diffusion) becomes restricted. Additionally, the intercalation potential of graphite material becomes more similar to that of metallic lithium, which can lead to the occurrence of metallic lithium plating [59,67,76]. Particularly for LFP and NMC cells, aggressive capacity degradation was observed in the low-temperature field. LTO cells, on the other hand, are less sensitive to low and high storage temperatures than NMC, LCO, LFP, and NCA cells. Among them, LCO batteries seems to be the most sensitive to low temperature and SoC changes compared to other batteries [73].

Cells stored at the same temperature age at different rates in various SoCs. Battery degradation can occur at high SoC levels, specifically at SoC levels above 80%. This is caused by an imbalance of ions and electrons across the electrodes and electrolyte, which can lead to a potential difference within the battery. This potential disequilibrium can promote side chemical reactions, resulting in battery degradation. Additionally, batteries are chemically stressed when they are maintained at a high SoC, causing degradation of the electrode materials over time [60,65–69,72,77]. During calendar aging, the accelerated aging tests focused on examining how temperature and the SoC affect cell performance in terms of capacity degradation [53,55,60,72]. The results showed that high SoC values not only speed up the aging process, but also capacity degradation effects are non-linear over time. Additionally, it was observed from the literature that the degradation rate remains relatively constant in the mid-SoC range [67,72].

The aging rate in NMC cells was found to increase at a 100% SoC, while NCA cells experienced an aging rate increase at SoC values above 90% [46,61,72]. Aging in LFP cells, on the other hand, is affected by SoC but not as significantly as in NMC and NCA cells [47]. In contrast, LCO chemistry degrades rapidly when the cell is charged and kept at a temperature of 40–50 °C. However, reducing the SoC slightly can significantly reduce the degradation rate. Comparing these results with LFP degradation rates, it is evident that LFP chemistry has a slightly lower degradation rate under the same conditions (high temperature and SoC). However, the degradation rate remains fairly constant despite changes in SoCs at a given temperature. Therefore, it can be concluded that temperature has a greater impact on degradation within LFP cells [52,62,75]. There is not as much of the literature available on the calendar aging of LTO-based cells compared to other types of batteries. However, it is understood that cells with LTO are less affected by temperature and the SoC than NMC and NCA cells. It is worth noting that LTO cells tend to degrade more quickly at a low SoC compared to a high SoC. This tendency could be due to the depletion of limited lithium inventory, particularly at low potentials [73].

In addition, when examining battery aging, larger lithium-ion cells may have different performance and aging patterns compared to smaller ones, even if they have the same cell chemistry. These distinctions stem from variations in factors like current density, design, geometry, temperature distribution characteristics (hot spot formation due to area/volume ratio variation), and the electrochemical reaction rate affected by design and spatial irregularities in electrical potential. For instance, in two studies conducted under similar conditions [54,55], the relative capacity of the 15 Ah LFP cell was 0.55 under 250-day 65 °C and 100% SoC storage conditions, while it was 0.68 for the 8 Ah capacity LFP cell.

2.2. Evaluation of Empirical/Semi-Empirical Calendar Aging Models

There are various mathematical models in the literature for predicting battery calendar aging, based on empirical evidence. These models can be divided into two categories: empirical and semi-empirical. An empirical formula is a mathematical expression or curve that best fits observations or measurements. However, they require experimental data and are only valid for specific operating conditions. This requirement can make it challenging to predict outcomes beyond the range of experimentation. Semi-empirical models, on the other hand, use a combination of theory and experimental data. For instance, if a theory predicts a linear relationship, the best linear relationship is found from the available data, even if the best fit curve is non-linear [38,39]. This study includes both empirical and semi-empirical models, with a greater emphasis on the latter, to improve understanding of semi-empirical studies. We will explore and elucidate the intricacies of these studies to ensure a comprehensive understanding of their methodologies.

A commonly used semi-empirical model, which follows the Arrhenius equation, has been extensively used in various studies to describe capacity degradation while in storage. As a result of the influence of storage temperature (T) on physical reactions, battery SEI growth can be elucidated through the Arrhenius law. This approach correlates temperature with chemical reaction rate. The literature shows that the Arrhenius equation agrees with aging rates, especially for calendar aging [39]:

$$Q_{loss} = A \times e^{-\frac{E_a}{RT}} t^z \quad (1)$$

In this equation, A represents the exponential factor, E_a represents the activation energy, R is the gas constant, T is the absolute temperature, and t represents time. SEI growth in lithium-ion batteries is often presumed to increase proportionally with the square root of time, aligning with basic models of diffusion-limited surface layer expansion. Therefore, z is typically assumed to be 0.5 [78,79].

To account for the effect of the SoC on calendar aging, some experimental studies incorporated the Arrhenius law by considering the correlation between temperature and

the SoC. According to Arrhenius's law, the degradation in calendar capacity can finally be expressed in a specific semi-empirical form as follows [38,47,52,61]:

$$Q_{loss} = f(T, SoC, t) \tag{2}$$

$$Q_{loss} = A(SoC) \times e^{-\frac{E_a(SoC)}{RT}} \times t^z \tag{3}$$

Both the exponential term A(SoC) and the activation energy E_a (SoC) in Equations (2) and (3) are SoC dependence terms. Recognizing that the effects of storage SoC on parasitic chemical reactions can lead to capacity degradation, studies have revealed both linear and exponential dependencies of the SoC [38,47,61,66,67]. These models establish mathematical relationships between capacity loss, temperature, and the SoC for the calendar life model. In a model created by Sarasketa-Zabala et al. [52], calendar aging is modeled as exponentially dependent on SoC, where T refers to the storage temperature, and t represents the storage time in days. The model's predictions closely matched the experimental results, with the model's error consistently below 1% during the entire experimental period. Hoog et al. [61] combined both empirical and semi-empirical models. The Arrhenius law establishes the correlation between temperature and calendar aging, whereas a linear empirical model is established for the SoC relation. The parameters a; b; c; and d in the formula are fitting parameters. In addition, Eddahech et al. [47] modeled SoC dependence as a polynomial function, accounting for the interdependence of temperature and the SoC through multiplication. The parameters $a_{1–3}$; $b_{1–3}$; c; and d in the formula are fitting parameters.

Another study [63] argued that the SoC drifts over time due to reversible and irreversible capacity losses (Q_{sd} and Q_L). The SoC is determined by the ratio of the amount of load (Q_a) available at a specific time (t) and the total capacity (Q). The aging model is based on Eyring's law by taking the pair (T, Q_a) as aging accelerating factors. While the prediction error of the model with SoC values as constant is 4.8%, the prediction error of the model with the SoC change taken into account is 2%.

In another study [38], a semi-empirical model that combines an exponential and a linear function following the Arrhenius law agrees well with measurements for all SoCs and temperatures. It was suggested that it reflects the aging process better than the commonly used square root dependence of time. The square root function tends to overestimate the capacity degradation at the beginning of aging and underestimate aging in the later period, especially when extrapolated.

In the literature, capacity loss models are typically represented as cumulative data extracted from experiments conducted under constant stress conditions (such as temperature and the SoC). However, in real-world scenarios such as electric transportation, stress conditions vary over time. In this reason, unlike other semi-empirical models, models based on the degradation rate were developed that take into account the capacity degradation over time [54,66,67], which are rooted from a simple empirical expression (4) to predict degradation under conditions of unstable stress levels.

$$\frac{dQ_{loss}}{dt} = k(T, SoC) \times \left(1 + \frac{Q_{loss}(t)}{C_{nom}}\right)^{-\alpha(T)} \tag{4}$$

where k(T,SoC) represents the capacity degradation evolution during storage with the effects of temperature and the SoC. $Q_{loss}(t)/C_{nom}$ is the fractional capacity degradation at aging time t. In the model documented in Grolleu et al. [54], the parameter k(T,SoC) demonstrates an exponential growth in response to temperature variations while concurrently exhibiting a linear relationship with the SoC. Su et al. [66] described the effect of temperature and the SoC on the k(T,SoC) parameter using a quadratic polynomial. This model accurately predicted capacity degradation with maximum errors of 1% for 240-day static storage and 3% for 180-day non-static storage.

Naumann et al. [67] developed a model for dynamic conditions that takes into account capacity degradation over time. After the aging model was developed, a differential form of the aging model was derived by differentiating the model concerning time to apply model equations with changing temperatures or SoCs over time. Temperature effect K(T,SoC) is governed by the Arrhenius law, while the SoC effect is governed by a cubic function. The model demonstrated absolute errors consistently below 2.2% against validation data points. These studies demonstrate that models can be developed with minimal errors under dynamic as well as static conditions.

In their research, Ecker et al. [28] compared various empirical model equations and concluded that their measurement data have little to no linear component. As a result, they chose to use a semi-empirical model due to its low root-mean-square-error (RMSE) and smaller number of coefficients for capacity, ohmic resistance, and polarization resistance. Their model uses the parameters of temperature, aging period, and potential, which is related to the SoC of the cell, which is as follows:

$$\frac{L(T,V,t)}{L(T_0,V_0,t_0)} = 1 + B(T,V) \times c_a t^{0.5} \quad (5)$$

The coefficient "c_a" is utilized to gauge the rate at which capacity losses occur under reference conditions T_0, t_0, and V_0. The value of L(T, V, t) provides an estimation of the resistance or capacitance at a particular time t with temperature T and voltage V. Furthermore, the effects of temperature and storage voltage are calculated according to an exponential dependence (6):

$$B(V,T) = C_v^{\frac{V-V_0}{\Delta V}} \times C_T^{\frac{T-T_0}{\Delta T}} \quad (6)$$

The reference temperature and voltage are represented by T_0 and V_0, respectively. D_T and D_V were set at 10 °C and 0.1 V, respectively, in their study based on arbitrary values. The proposed law (6) utilizes c_T and c_V parameters, which are determined by analyzing the results of accelerated calendar aging tests. It is assumed that the degradation rates were 1/2 dependent on time, based on their data.

Similarly, Schmalstieg et al. [60] takes a comparable approach, utilizing the Arrhenius equation to account for temperature dependency of aging and a linear relationship to describe voltage dependency. However, they use a modified version of the square root with an exponent of 0.75 to account for time dependency.

The models used in electric vehicle batteries discussed above are summarized in Table 2, highlighting their key elements. These models vary in the stressors they consider, such as time, storage temperature, the SoC, and in the outcomes of the aging type they examine. It should be noted that empirical and semi-empirical methods measure a battery's available capacity under reference conditions throughout its lifespan, eliminating variations in the available capacity caused by various operating conditions.

Table 2. Overview of semi-empirical/empirical calendar aging model equations reported in the literature.

Source	Model Cases	Type of Result (%)	Model Equation	Model Parameters	Model Error (%)
Wang et al. [39]	SEM	Capacity Loss	$A \times e^{-\frac{E_a}{RT}} t^{0.5}$	Temperature and time	5%
Redondo-Iglesias et al. [63]	SEM	Capacity Loss	$A \times e^{b.SoC} \times e^{\frac{-E_a + c \times SoC}{kT}} \times t^z$	Temperature, SoC shift, and time	Max. Error 2
Sarasketa-Zabala et al. [52]	SEM	Capacity Loss	$A \times b \times \exp(cT^{-1}) \times \exp(dSoC) \times t^{0.5}$	Temperature, SoC, and time	0.9%
Eddahech et al. [47]	EM	Remaining Capacity	$({}_1SoC + a_2T + a_3T \times SoC) \times e^{(b_1SoC + b_2T + b_3T*SoC) \times t} + ce^{dt}$	Temperature, SoC, and time	-
Werner et al. [38]	SEM	Remaining Capacity	$1 + a\langle SoC, T\rangle \times (\exp(-b\langle SoC, T\rangle \times t) - 1) + c\langle SoC, T\rangle \times t$	Temperature, SoC, and time	RMSE 0.12–0.15

Table 2. *Cont.*

Source	Model Cases	Type of Result (%)	Model Equation	Model Parameters	Model Error (%)
Hoog et al. [61]	SEM-EM	Capacity Loss	$A \times e^{-\frac{Ea}{RT}} t^z / (a_1 T^{a_2} \times a_3 t^{b_1 T^{b_2} \times b_3} \times SoC^{c_1 \times T^{c_2}}) + (d_1 \times T^{d_2} \times d_3 \times SoC \times t)$	Temperature, SoC, and time	RMSE 5
Grolleu et al. [54]	SEM	Capacity Loss	$k_A \times \exp\left\{-\frac{Ea_A}{R}\left(\frac{1}{T}-\frac{1}{T_{ref}}\right)\right\} \times SoC + k_B \times \exp\left\{-\frac{Ea_B}{R}\left(\frac{1}{T}-\frac{1}{T_{ref}}\right)\right\} \times \left(1+\frac{Q_{loss}(t)}{C_{nom}}\right)^{-\alpha(T)}$	Temperature, SoC, and time	3–4%
Su et al. [66]	SEM	Remaining Capacity	$a + b\frac{T-52.5}{7.5} + c\left(\frac{T-52.5}{7.5}\right)^2 + d\frac{SoC-0.6}{0.2} + e\left(\frac{SoC-0.6}{0.2}\right)^2 + f\frac{T-52.5}{7.5} \times \frac{SoC-0.6}{0.2} \times \left(1+\frac{Q_{loss}(t)}{C_{nom}}\right)^{-\alpha_0 \exp(\frac{\lambda}{T})}$	Temperature, SoC, and time	3%
Naumann et al. [67]	SEM	Capacity Loss	$k_{ref,Qloss} \times \exp\left\{-\frac{Ea_{Qloss}}{R}\left(\frac{1}{T}-\frac{1}{T_{ref}}\right)\right\} \times \left(C_{Qloss}(SoC-0.5)^3 + d_{Qloss}\right) \times \left(2\sqrt{t}\right)^{-1}$	Temperature, SoC, and time	2.2%
Ecker et al. [28]	SEM	Remaining Capacity	$1 + C_a \times C_v^{\frac{V-V_0}{\Delta V}} \times C_T^{\frac{T-T_0}{\Delta T}} \times \sqrt{t}$	Temperature, voltage, and time	0.7–1%
Schmalstieg et al. [60]	SEM	Remaining Capacity	$1 - (C_{v1}V - C_{v0}) \times 10^6 \times \exp\left(-\frac{C_T}{T}\right) \times t^{0.75}$	Temperature, voltage, and time	1.2–1.7%

3. Cyclic Aging

Battery cyclic aging in electric vehicles is a critical consideration in their long-term performance and reliability. Cycling corresponds to the irreversible capacity degradation that occurs during the charging and discharging of a battery. In addition to temperature and the SoC, various other stress factors become pertinent during cycling, including the rate of discharge or charge, often referred to as the C-rate, and the SoC ranges (ΔSoC) throughout a cycle [80–82]. The ΔSoC represents the degree of variation in SoC experienced during a single cycle. This section aims to explore various studies in the literature that have produced noteworthy findings on the subject of battery cycling aging.

Han et al. [16] tested different cell types, subjecting them to charging and discharging cycles at different temperatures. They found that while the LTO/NMC cell showed minimal capacity loss and negative electrode material degradation, there was noticeable loss of NMC positive electrode material. LMO and LFP cells experienced lithium inventory and negative electrode material loss, with LFP cells losing 20% capacity in 200–300 cycles and LMO cells showing decline around 420 cycles. Yang et al. [83] explored the impact of temperature differences among parallel-connected cells on unbalanced discharging and aging using LFP cells. Using the Arrhenius approach, they estimated capacity degradation. Their findings suggest that minimizing temperature differences among cells in parallel connection is essential for extending battery life, as increased temperature differences correlate with increased capacity loss. Baghdadi et al. [84] conducted a cycling study on LMO + NMC and NCA cells, considering temperature, the SoC, and current effects on aging. They used a chemical ratio approach based on the Dakin degradation model and found that aging rate increases exponentially with a higher SoC, temperature, and current [85]. Lower temperatures accelerated overall aging, with a significant increase in aging rate observed between −5 °C to 25 °C and 25 °C to 60 °C ranges. Hoog et al. [61] documented a lifetime model for an NMC cell for the automotive industry. The paper highlights that capacity loss was notably affected by a 100% DoD and temperature in cycling aging experiments.

Wu et al. [86] studied the impact of low temperatures and cycling charging on battery degradation using 5 Ah LFP batteries. They found significant degradation of up to 35% at temperatures of −10 °C and −20 °C, where lithium-ion losses transformed into lithium plating, forming dendrites that increased ohmic resistance and decreased capacity. Burow et al. [87] investigated the aging of 25 Ah prismatic NMC Li-ion cells at low tem-

peratures (5–20 °C), observing capacity loss after the 200th cycle. Post-mortem analysis revealed that primary aging was due to lithium plating, with non-homogeneous distortion observed at the negative electrode.

In another study conducted at low temperatures, Rauhala et al. [88] explored challenges in deploying large lithium-ion battery systems in cold climates, focusing on the reduced cycle life of LFP cells at low temperatures. Their findings suggested that at 0 °C, both lithium plating and SEI growth were observed on the graphite electrode, whereas only lithium plating occurred at −18 °C.

Todeschini et al. [89] developed a capacity degradation model for LFP batteries, validated through experiments. They observed significant aging at a 0–30% SoC and eight C-rate, with capacity decreasing to 80% after 4000 cycles. They proposed a semi-empirical model linking the SoC and C-rate to predict capacity degradation, with an average error rate of 0.24% compared to experimental data. Cordoba-Arenas et al. developed [90] a semi-empirical cycle life model for 15 Ah LMO + NMC cells based on insights gained from 16 cycling experiments conducted over 3 months. They varied minimum SoC levels, while considering charge sustaining/depleting ratios. Plug-in Hybrid Electric Vehicles (PHEVs) can operate in two modes according to the United States Advanced Battery Consortium (USABC): Charge-Depleting (CD) and Charge-Sustaining (CS). They distinguished between Charge-Depleting (CD) and Charge-Sustaining (CS) modes. The CD mode drains the battery from maximum to minimum SoC for electric and hybrid driving, while the CS mode maintains a stable SoC range for hybrid operation. Results showed that capacity degradation rate increased with higher minimum SoC values, especially when exceeding 35%.

Lithium-ion batteries are used in various applications for energy storage and may not always experience complete charging and discharging cycles. Saxena et al. [91] studied the impact of partial charge–discharge cycles on capacity loss in 1.5 Ah LCO pouch cells. The study uses equivalent full cycles (EFCs) to evaluate cycle life performance due to incomplete cycles caused by partial SoC intervals in cells. Findings revealed that average SoC values during the initial 500 full cycles significantly influenced cell disruption, while ΔSoC intervals between 600 and 800 cycles had a greater impact on degradation. Then, they developed a model of battery degradation based on partial and full charge cycles. The model describing this degradation is based on the power law model [92,93], which is compatible for the full number of cycles in the first 500 cycles. In another study using EFCs, Gao et al. [94] performed experiments at various SoC ranges and identified lithium loss as the primary aging mechanism in batteries below 20% DoD. Also, Gantenbein et al. [95] performed cycling experiments at various SoC ranges, primarily with NCA cells, and the 65–85% SoC range showed maximum capacity and active lithium-ion loss.

Wikner and Thiringer [96] investigated the impact of aging at different SoC levels in electric vehicle 26 Ah LMO + NMC cells over three years. They varied SoCs at 10% intervals, different temperatures, and C-rates, developing an empirical battery model based on observed degradation. Their findings highlighted that reducing the SoC to 50% could increase battery lifetime by a range of 44–130%, especially for high SoCs and discrete driving types. Batteries with high SoCs and various C-rates experience accelerated aging relative to high C-rates for a given SoC. Benavente-Araoz et al. [97] conducted comprehensive aging tests on NCA lithium-ion cylindrical cells, varying cut-off voltages, and SoC ranges over multiple cycles. They found that high cut-off voltages and a wide ΔSoC (20% to 95%) led to severe material degradation and electrode shift, while high cut-off voltage with a narrow ΔSoC (65% to 95%) caused greater electrode degradation but minimal cell unbalance.

Preger et al. [98] conducted a multi-year cycling investigation involving LFP, NCA, and NMC cells at various SoC values, temperatures, and C-rates. They found that NCA and NMC cells experienced more pronounced capacity degradation as they transitioned from partial to complete SoC, attributed to their higher operating voltages promoting electrolyte oxidation. NCA and NMC cells also exhibited rapid capacity degradation when operated at 100% SoC, while LFP cells demonstrated significantly longer cycle life spans

under tested conditions. Naumann et al. [99] conducted a 29-month study on cycling aging of lithium-ion cells, focusing on 2.85 Ah LFP cells under different conditions including temperature, C-rate, depth of cycle (DoC), and SoC_{mean}. They found that capacity loss was strongly affected by the DoC and SoC, with a lower DoC initially leading to higher rates of capacity degradation. A larger DoC led to higher ultimate capacity losses at higher cycle numbers, as expected. A semi-empirical model was developed based on the static cycle aging study to predict capacity loss for the influence of C-rate, DoCs, and Ah-throughput.

Wang et al. [92] developed a cycle-life model to study capacity degradation in LFP batteries. They conducted extensive cycle tests exceeding 2000 cycles on 2.2 Ah LFP cells, varying temperatures, DoDs, and discharge rate. Results showed that at higher C-rates, the impact of charge/discharge rates became more significant, with noticeable cell heating observed during cycles involving high discharge rates. In another study conducted by Wang et al., they focused on tests related to the aging cycle of NMC + LMO cells [39]. Lower temperatures and higher C-rates were found to increase mechanical breakdown and cycle life loss in the experiments. Their results are shown in Figure 4. Two cells were tested under each set of conditions, which included four different temperatures (10 °C, 22 °C, 34 °C, and 46 °C), five DoD levels (90%, 70%, 50%, 30%, and 10%), and five discharge rates (C/2, 2 C, 3.5 C, 5 C, and 6.5 C). A 1 C discharge rate corresponds to a current of 1.5 A. For all the cells, the cycle test cut-off voltages were set at 4.2 V and 2.5 V. At 10 °C, capacity degradations notably occurred with C-rate, while the difference in capacity between temperatures of 34 °C and 43 °C diminished, indicating reduced C-rate dependence. This dependence is attributed to induced voltages during fast discharge at the negative graphite electrode, particularly when lithium diffusion kinetics are inhibited at low temperatures. Similarly, Omar et al. [75] conducted experiments on 2.3 Ah LFP batteries to study cycle aging under various conditions, including different current rates, operating temperatures, and discharge depths up to 3000 cycles. They found that higher current rates, especially at 15 C, significantly limited the battery's cycle life to only 560 cycles.

Sarasketa-Zabala et al. [100] performed cyclic tests on 2.3 Ah LFP cells, examining various C-rates and DoD values while developing a semi-empirical model. They found that static cycling had a greater impact on cell behavior than dynamic operation. When cycling at a low 10% depth of discharge, the duration of cycling (measured in Ah-throughput) emerged as a more influential factor than the C-rate. Interestingly, at a low 10% DoD, the duration of cycling was more influential than the C-rate, while at a 60% DoD, the C-rate's influence increased, contrary to conventional theory. Groot et al. [101] conducted a comprehensive study on the cycle life of LFP cells, examining various charging and discharging C-rates. Their research aimed to quantify aging in terms of capacity loss under conditions typical of high-power automotive applications. They found that faster degradation occurred when cells underwent fast charging coupled with slow discharging compared to symmetric cycling. Wu et al. [102] investigated battery aging in 5 Ah LCO + NCA pouch cells, focusing on discharge rates (1 C, 2 C, 3 C) and temperatures (10 °C, 25 °C, 40 °C). Their study revealed higher sensitivity to low temperatures but lower sensitivity to discharge rates compared to prior research. Sensitivity to low temperature is due to positive electrode deterioration. Despite high discharge rates up to 5 C, these cells could endure 3000–5000 cycles before experiencing a 20% capacity degradation, suggesting efficient capacity utilization due to reduced thermal and mechanical stress in their geometry.

Petit et al. [103] developed an experimental cyclic capacity model for 2.3 Ah NCA and LFP cells, considering factors like temperature and current for cycling aging. In addition to other studies, they observed that prolonged exposure of batteries to a high SoC resulting from fast charging also increases capacity loss. Their study showed that NCA batteries were more susceptible to cyclic aging and aged earlier under high charge rates compared to LFP batteries.

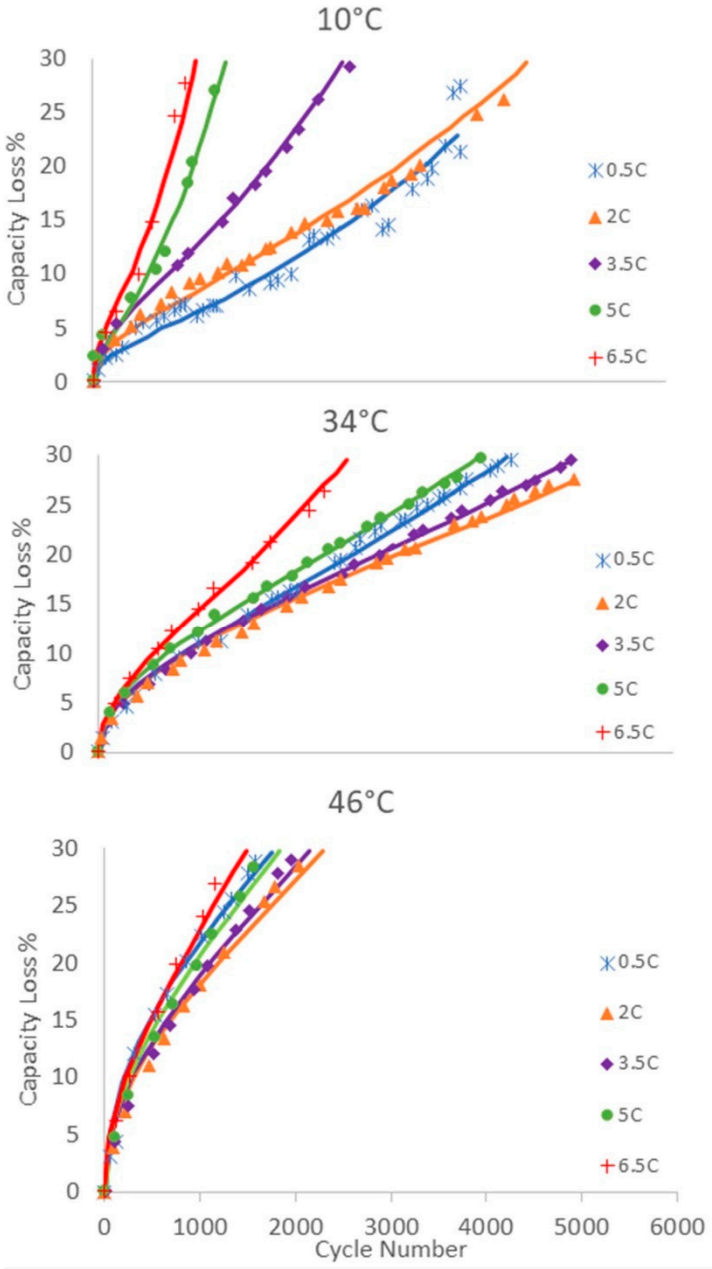

Figure 4. In the study conducted by Wang et al. cycling capacity loss at different temperatures (10 °C, 34 °C, and 46 °C, respectively) for different discharge rates (0.5 C, 2 C, 3.5 C, 5 C, 6.5 C) [39].

Barcellona and Piegari [104] analyzed the aging of 10 Ah LCO Peltier cells, concerning cycling aging's dependency on the current rate. Their findings suggested that capacity degradation remains independent of the current rate for moderate rates (up to 5 C) and initial capacities of up to 95%, provided that the battery temperature is within the appropriate range and the cell avoids excessive voltage stress. Saldana et al. [105] investigated a 63 Ah NMC battery cell in a commercial electric vehicle and presented a simple but realistic degradation model. Their findings emphasized that, besides temperature, the C rate exerted the most substantial influence on battery degradation, while the DoD showed a linear relationship with degradation, particularly concerning capacity loss. Krupp et al. [106] introduced a semi-empirical cyclic battery aging model focusing on graphite negative electrode mechanisms like SEI cracking and active material cracking. The model distinguishes between aging mechanisms, showing negligible current rate dependence on SEI growth but strong dependence on active material cracking. The total capacity loss predicted by the model is

lower than the actual measured data from the dynamically cycled cell, with a mean average deviation of 0.2%. Kucinskis et al. [107] tested various battery cells (NCA + LNO and NMC) and electrode materials, using Arrhenius plots to identify crossover temperatures indicating shifts in aging mechanisms. Higher charging rates generally increased crossover temperatures, while electrode characteristics showed complex correlations with aging behavior. Thinner electrodes with smaller particles exhibited lower crossover temperatures, suggesting reduced susceptibility to lithium deposition, especially in high-power cells.

Cycling lithium-ion batteries causes capacity degradation and changes in the open-circuit voltage curve due to the loss of LAM and LLI. Karger et al. [108] devised an empirical calendar aging model addressing capacity degradation and open-circuit voltage curve changes in cycling lithium-ion batteries. Using data from 2.0 Ah NCA batteries, they identified stress parameters leading to active material and loss of lithium inventory. The model greatly improves OCV curve predictions, increasing voltage accuracy eightfold compared to non-updated curves.

3.1. Evaluation of Empirical Cyclic Aging Studies

Cyclic aging in EVs refers to the gradual deterioration of the batteries over time due to repeated charge and discharge cycles. Cycling aging impacts several critical parameters, including capacity, voltage, internal resistance, state of charge range, and overall performance. Over time, the battery's ability to store energy diminishes, reducing the driving range and affecting power delivery. Internal resistance increases, slowing down charging and decreasing efficiency. This phenomenon is primarily associated with the use of lithium-ion batteries, which are common in EVs, and several parameters influence cycling aging. The primary factors include the number of charge and discharge cycles that the battery undergoes, the range of the SoC during these cycles, the operating temperature, and the charging and discharging rates. The cumulative effect of these factors leads to capacity degradation, where the battery can store less energy over time, reducing the EV's driving range. As detailed in Section 3, various experimental studies in the literature have explored the impact of these parameters on cycling aging behavior. Cycling aging behaviors can be interpreted differently depending on the parameters studied. For example, while some studies investigate the impact of combining temperature and the SoC, other studies propose correlations between aging and the combination of temperature and C-rate. In order to provide a comprehensive overview of the research conducted, a summary of the examined studies has been meticulously compiled in Table 3.

Battery cycle aging can occur during both charging and discharging. It is caused by various factors such as the battery's capacity, usage patterns, temperature conditions, and current demands. Additionally, the factors mentioned in calendar aging also apply to studies of cyclic aging, as they have a similar impact on battery performance. These aging phenomena occur during both batteries are in use and at rest; thus, this article will delve deeper into the C-rate and ΔSoC (or SoC_{mean}) factors that contribute to cycling aging, in addition to the factors already discussed in calendar aging.

The factors that contribute to cycling aging are dependent on the usage mode of the battery. One of the most commonly cited factors in research is the ΔSoC, which reflects the changes in the load state during a cycle. This factor primarily takes into account the amount of charge that the battery receives (or discharges) during a cycle. Studies showed that high ΔSoC values lead to accelerated capacity loss, regardless of other conditions. This outcome is mainly due to the degradation of the positive electrode and the development of the SEI caused by high discharge or charge [95,96].

Table 3. Overview of cycling aging for EVs studies reported in the literature, with study conditions and experimental data.

Study	Chemistry	Capacity (Ah)	Number of Cycle	EFC	Parameters			
					Temp. (°C)	ΔSoC (%)	DoD (%)	C-Rate (C)
Han et al. [16]	LTO + NMC, LMO and LFP	20, 35, and 10, 60 and 11	1000	-	5 and 45	-	-	1.5
Preger et al. [98]	LFP, NCA, and NMC	1.1, 3.2, and 3	-	2500–9000, 250–1500, and 200–2500	15, 25, and 35	40–60, 20–80, and 0–100	0–100, 20–80, and 40–60	0.5, 1, 2, and 3
Petit et al. [103]	NCA and LFP	7 and 2.3	4000	-	5–30	-	-	0.16–4 C
Baghdadi et al. [84]	LMO + NMC and NCA	5.3 and 7	-	-	40, 45, and 50	20, 30, and 40	-	1 and 2
Wang et al. [39]	LMO + NMC	1.5	2000–5000		10, 22, 34, and 46	-	10	0.5, 2, 3.5, 5, and 6.5
Wikner and Thiringer [96]	LMO + NMC	26	-	2000–10,000	25 and 35	0–10, 0–30, 10–20, 20–30, 40–50, 60–70, 70–80, and 80–90	10, 20, 30, 40, 50, 60, 70, 80, and 90	1, 2, and 4
Cordoba-Arenas et al. [90]	LMO + NMC	15	-	-	10, 30, and 45	25, 35, and 45	-	0.33, 0.75, and 5 C
Wu Yao et al. [102]	NCA + LCO	5	-	3000–6000	10, 25, and 40	50	-	1, 2, and 3
Kucinskis et al. [107]	NCA + LNO and NMC	5 and 0.1	50–662	-	−15–60	-	-	0.2, 0.4, and 0.6
Yang et al. [83]	LFP	2.2	1000	-	25 and 40	-	75	3 C
Wu et al. [86]	LFP	2.3	40–100	-	−10 and −20	0–100%	-	0.3–0.5
Rauhala et al. [88]	LFP		-	-	−18, 0, and 25	-	-	1
Todeschini et al. [89]	LFP	2.3	4000–14,000	-	55	0–10 and 0–30	-	2, 4, and 8
Wang et al. [92]	LFP	2.2	0–10,000	-	0, 15, 45, and 60	-	10–90	0.5, 2, 6, and 10
Omar et al. [75]	LFP	2.3	1500–3000	-	−18, 0, 25, and 40	-	20, 40, 60, 80, and 100	1, 5, 10, and 15
Sarasketa-Zabala et al. [100]	LFP	2.3	-	2000–6000	30	50	5, 10, 30, 50, 60, and 100	1, 2, and 3.5
Groot et al. [101]	LFP	2.3	600–4800	-	23–53	60–100	60 and 90	1–4
Naumann et al. [99]	LFP	2.85	-	2000–14,000	25 and 40	25, 50, and 75	-	0.2, 0.5, and 1
Hoog et al. [61]	NMC	20	3000	-	25, 35, and 45	35, 50, 65, and 80	20–100	0.33, 1, and 2
Burow et al. [87]	NMC	25	500	-	5 and 20	0–100	-	1
Gao et al. [94]	NMC	8	-	2800–3400	25	0–20, 20–40, 40–60, 60–80, 8–100, and 0–100	20	6
Saldana et al. [105]	NMC	63	1800	-	25 and 45	-	20, 40, 60, and 80	0.3786, 0.4812, and 0.6710
Krupp et al. [106]	NMC	64	-	800	23	50, 70, and 90	0–100	2
Gantenbein et al. [95]	NCA	2.6	4000	-	25	5–25, 25–45, 45–65, 65–85, and 75–95	20	1
Benavente-Araoz et al. [97]	NCA	2.5	700–1000	-	25	65–95, 35–65, 20–50, and 20–95	-	0.1
Karger et al. [108]	NCA	2.0	-	2500	5, 20, 35, and 50	-	20–100	0.5–2
Saxena et al. [91]	LCO	1.5	-	800	25	0–100, 20–80, 40–60, 40–100, and 0–60	-	0.5 and 2
Barcellona and Piegari [104]	LCO	10	-	-	20–30	20–80	-	0.8, 2.5, and 5

Studies showed that the lowest cycling aging occurs at a SoC_{mean} of around 50%, which is within a 40–60% ΔSoC. On the other hand, the highest cyclic aging occurs at a SoC_{mean} of 95%, which is within a 90–100% ΔSoC. The impact of the SoC may vary depending on the different stages of lithiation of the graphite negative electrode. When the graphite negative electrode charges, it expands in volume, and when it discharges, it retracts. This expansion and retraction are more noticeable during the switching of lithiation stages. Cycling between these stages can lead to an increased particle cracking and the formation of a new SEI. Furthermore, in every SoC range, Li-ion loss occurs due to the dominant aging mechanism [97].

At higher ΔSoC levels, LMO cells experience an accelerated aging process. In batteries featuring a graphite negative electrode, Mn^{2+} ions may migrate towards the negative electrode and undergo reduction on its surface, as the graphite negative electrode has a low potential. These ions catalyze the thickening of the SEI film, which causes a reduction in battery capacity and an increase in resistance [16,96,109]. Studies on cycling aging showed that NMC and NCA cells are more susceptible to SoC range cycling compared to LFP cells [94,95,98,99]. LTO chemistry is also more resistant to calendar aging than other battery chemistries when the state of charge is kept at medium to high levels [16]. LCO cells degrade rapidly at high SoCs and temperatures of 40–50 °C, with SoC changes having the biggest impact for degradation.

One factor that affects the lifespan of a lithium-ion battery and its functionality is the rate of charge and discharge it undergoes over time. The main cause of aging from this factor is positive electrode degradation and the development of an SEI due to high discharge or charge. Secondly, the increased stress on the battery's materials, particularly the electrode materials, can lead to mechanical wear and tear, further deteriorating the battery's performance over time. Inferences regarding C-rate-dependent degradation can be interpreted from many studies with different chemistries. One type of battery, LFP cells, are known for their capacity to handle high amounts of power but also the literature shows that LMO cells have a longer life than LFP cells, which is consistent with the observed cycling trends [92]. The aging process of LMO cells is sped up when they are discharged to a lower potential at high rates. This process happens because LMO cells typically exhibit faster lithium-ion diffusion rates during discharge compared to LFP cells, which contributes to their higher power capability [39]. Li-ion cells that use LTO negative electrodes have the ability to sustain extremely high C-rates with minimal degradation. This is primarily because LTO is a 'zero-strain' material, meaning it undergoes negligible volume change during charging and discharging cycles. Unlike other negative electrode materials that expand and contract during these cycles, LTO remains structurally stable, which contributes to its longevity and durability. This stability comes at the cost of lower energy density due to their higher potential. Additionally, studies showed that NCA cells are more susceptible to aging under high C-rates. However, when conducting cyclic aging tests, it is important to consider the impact of energy density on the C-rate. The most suitable cell chemistries for applications requiring high C-rates at room temperature are LFP and NMC, followed by LTO, NCA, and LCO cells [89,91,104,105].

To properly explain how the C-rate affects battery performance, it is important to distinguish between temperatures above and below the desired temperature range. In one study [102], it was found that increasing the C-rate from 0.5 C to 2 C had little effect at 40 °C but had a noticeable effect at 25 °C, indicating that temperature affects C-rate. The authors suggested that the higher reaction rate and ion diffusion kinetics at these temperatures may decrease the stress caused by the increased C-rate. When the temperature is lower, the conductivity of ions and the rate of intercalation decrease. On the other hand, a higher C-rate leads to faster diffusion kinetics and, therefore, higher current density. This increase means that at lower temperatures, the harmful effects of an increased C rate are accelerated, leading to more mechanical and kinetic stress on the electrodes and a greater polarization gradient. This outcome can ultimately result in lithium plating. However, even at higher temperatures, the C-rate can still cause structural damage, such as crack

propagation in the SEI layer, overloading of the positive electrode resulting from the increased polarization gradient, or the exfoliation of graphite at the negative electrode and positive electrode [27,110]. The authors suggested that the higher reaction rate and ion diffusion kinetics at these temperatures may decrease the stress caused by the increased C-rate.

The graph presented in Figure 5 depicts the capacity degradation versus significant interactions for three specific chemistries tested at 200 EFC [98]. It is important to note that different chemistries exhibit varying levels of dependence on different variables, and it is not advisable to draw general conclusions about variable dependence across different chemistries. The average % capacity refers to the average value for all cells under specified conditions at 200 EFC. Figure 5a illustrates that the capacity degradation is more affected by the C-rate for NMC and NCA cells compared to LFP cells. On the other hand, Figure 5b shows that the capacity degradation for NCA and NMC cells is affected similarly by the SoC spacing, with a 5% to 10% decrease observed at a range of 0% to 100%. However, the SoC has little effect on the capacity of LFP cells. Moreover, temperature affects the capacity degradation of NMC and LFP cells in opposite trends, as shown in Figure 5c. NMC cells show a less systematic trend between 15 and 35 °C.

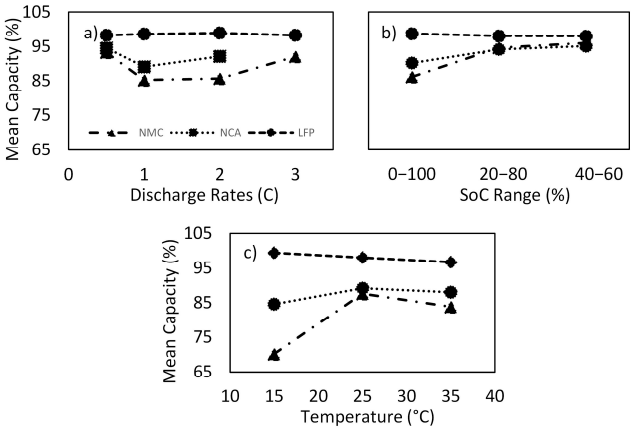

Figure 5. Main factors with 3 different battery chemistries ((**a**) Discharge Rates, (**b**) SoC Range, and (**c**) Temperature plots) for aging model [98].

In summary, cells with different chemistries for calendar and cyclic aging modes may exhibit divergent susceptibility to stressors affecting aging. Table 4 shows a qualitative comparison of the effects of stressors on different cell chemistries for both types of aging modes.

Table 4. Effect of stress factors on aging for cell chemistries for both aging modes. (●●●●: highest impact, ●●●: high impact, ●●: medium impact, ●: low impact).

Parameter	Cell Chemistry						
	LFP	NMC	NCA	LMO	LCO	LTO	LMO + NMC
Low SoC/ΔSoC	●	●	●	●	●	●●	●
Low C-rate	●	●	●	●	●	●	●
Low Temperature	●●	●●	●	●	●	●	●
Medium SoC/ΔSoC	●	●	●	●	●	●	●●
Medium C-rate	●	●●	●	●●	●	●	●●
Medium Temperature	●	●●	●	●	●●	●	●
High SoC/ΔSoC	●●	●●●	●●●	●●●●	●●●●	●●	●●●
High C-rate	●●	●●●●	●●●	●●	●●●●	●●	●●●
High Temperature	●●	●●●●	●●●	●●●	●●●	●●	●●●●

3.2. Evaluation of Empirical/Semi-Empirical Cycling Aging Models

Semi empirical cell aging models use limited data from cycled and stored cells under accelerated aging conditions. Cycle aging is more difficult to predict as it involves various independent variables such as temperature and current voltage. Moreover, these variables are linked to external conditions and battery usage. The primary factors taken into consideration are temperature, cycle number, ΔSoC, and C-rate. Cyclical aging models have varying structures and stressors relative to calendar aging models. Generally, cyclic aging models utilize either the cumulative charge efficiency (Ah-throughput) or the total number of equivalent full cycles (EFCs) to represent the battery cycle [105].

The EFC is employed to categorize any cycle or charge/discharge event based on the charge throughput of a full cycle. Cycle quantity is typically determined by scaling the EFC of the battery capacity (Q) with the total charge efficiency (C_{batt}) in Ah. The EFC is defined as the number at which the charging efficiency of a cell is twice its rated capacity, as shown in Equations (7) and (8):

$$Q = \int_0^t |I(t')|dt' \tag{7}$$

$$EFC = \frac{Q}{2 \times C_{batt}} \tag{8}$$

Here, *I* represents the charge–discharge current. Multiple definitions of C_{batt} exist, including nominal battery capacity at the beginning of life and present degraded battery capacity.

The term "Ah-throughput" refers to the amount of Ah that the battery delivers over multiple cycles. Throughput is often modeled using a power law relationship, similar to calendar aging (9). Additionally, throughput can also be associated with the number of cycle parameters (10):

$$Q = f(SoC, T, DoD, I)Ah^z \tag{9}$$

$$Q = f(SoC, T, DoD, I)N^z \tag{10}$$

Ah represents the total amount of energy delivered by the cell, N is the number of cycles performed, often expressed in terms of depth of discharge. Batteries cycled at higher DoDs degrade faster and have shorter lifespans. This relationship is often expressed using a power law model, where the total energy delivered by the battery, the number of cycles, and the depth of discharge are linked by an exponent 'z'. Studies modeling the effect of throughput on cyclic aging often relates Ah^z with $0.5 \leq z \leq 1$, where z is typically associated with the growth of an SEI layer.

Wang et al. [92] uncovered a power law correlation between battery capacity loss and charge throughput and developed a cycle life model based on it. Their equation shows that capacity loss follows a power law relationship with time or load flow, while an Arrhenius correlation accounts for temperature effects. In addition, it is widely accepted that the Arrhenius law applies to the effect of temperature on the reaction rate for most chemical processes for cycling aging, just as in calendar aging [60,61,68,92,111]. They created a battery life model that considers Ah throughput (time), C rate, and temperature, which is a generalized model. An empirical cycle aging model was developed, with predicted capacity loss values generally within ±5% of measured data. Additionally, their results uncovered that capacity degradation is dependent on $Ah^{0.55}$, which is directly proportional to aging time. This parameter allows degradation to be correlated based on C-rates. According to the article, Ah-throughput can be defined as

$$Ah = (\text{cycle number}) \times (DoD) \times (\text{full cell capacity}) \tag{11}$$

Wang et al. [39] proposed a new life model by merging the calendar and cycling models. In their model, capacity degradation has an exponential relation with C-rate and a linear relation with time (or charge throughput). They obtained a highly effective

empirical model that uses both an exponential and a quadratic polynomial relationship for temperature.

In another study on the cyclic aging model using Ah-throughput, Sarasketa-Zabala et al. [100] developed a semi-empirical model for dynamic conditions. They established mathematical relationships to connect the DoD and charging efficiency in the cycle life model. Their model showed an RMSE of 1.75% under dynamic cycling conditions.

They used two different equations in their aging modeling: one equation for DOD values between 10% and 50%, and another equation for all other DOD values. The cycling performance loss as a function of Ah-throughput differed depending on the DoD level ($Ah^{0.87}$ or $Ah^{0.65}$). However, the only challenge in applying this cycle life model is that the SoC release during charge and discharge (DoD) is assumed to always occur around a mid-SoC of 50%.

The capacity degradation can be expressed as a function of either Ah or n, based on the one-to-one relationship between total ampere-hours throughput and total aging cycle. Unlike most studies in the literature, instead of representing capacity degradation as a function of Ah-throughput, Todeschini et al. [89] used a power law fitting curve to express it as a function of n. The representation is as follows:

$$C_{f,i}(n) = a^i \times n^{b_i} \tag{12}$$

The estimated capacity value of the i-th battery after n aging cycles is represented by $C_{f,i}(n)$, and it is obtained from fitting data as a_i and b_i. A model was created to simulate the usage of low-charged batteries during the charging process. They uncovered that the most accurate curve fit was achieved with $n^{1.36}$, using an exponential factor greater than one because of the battery's quick decline in charge.

A semi-empirical cyclic aging model was developed by Cordoba-Arenas et al. [90]. This research considered the amount of time that a vehicle spends in Charge-Depleting (CD) and Charge-Sustaining (CS) modes when assessing the capacity loss caused by cell cycling. The ratio between CD and CS modes is defined by the following equation and ranges from 0 to 1:

$$\text{Ratio} = \frac{t_{CD}}{t_{CD} + t_{CS}} \tag{13}$$

where t_{CD} represents the duration in CD mode, while t_{CS} indicates the duration in CS mode. The sum of these durations, denoted as (t_{CD} + t_{CS}), represents the total study time. The ratio of the CD mode to the total runtime is then determined by dividing t_{CD} by (t_{CD} + t_{CS}). This equation for capacity degradation relies on the temperature of the battery during active phases, its minimum SoC level, and the Ah-throughput. The power law factor z, which represents the aging time, is taken as 0.48 in this equation. The battery's minimum SoC is determined by calculating the average SoC before each charging event. Their capacity degradation model exhibited a nearly perfect fit with experimental data, with an RMSE of 0.0047%.

In another study [99], it was aimed to create a unified aging model by superimposing a calendar aging and cyclical aging model. They considered the impact of C rate; DoC; and EFC yield on aging in their models. In the literature, DoC is also commonly referred to as depth of discharge (DoD or ΔDoD). They argued that the EFC for capacity loss, different C rates, and the DOC for all cycle aging tests follow an approximately square root dependence. One of the limitations of the model is that it does not account for the SoC stress factor in cyclic aging.

Saxena et al. [91] created a power law model that takes into account different SoC ranges to demonstrate how partial charge–discharge cycles can impact battery aging. The model shows that battery degradation is impacted not only by the average SoC, but also by the change in SoC (ΔSoC) during cycling. The model considers three different parameters at a constant temperature and C-rate: the average SoC, ΔSoC, and EFC.

Most studies on cycling aging utilize the Arrhenius equation, as well as a power law relationship for efficiency or number of cycles, described in the models above. This form of

modeling is often well suited to predicting aging due to cycling during post-processing computation. However, for online calculations over a shorter period or under rapidly changing operating conditions, the current age of the battery is often not taken into account in each new calculation. This situation was addressed by Petit et al. [103] with cycling aging modeling using the Arrhenius/power law. A similar approach was proposed by Wang et al. [92], which they employed for analyzing cycling aging. The study focused on temperature and current as stress factors for cycling aging. This expression is differentiated with respect to time to assess the incremental change in capacity due to cycling aging. The study demonstrated strong agreement between experimental results and simulations, with errors of less than 5% for capacity loss below 20%.

In studies based on Arrhenius and power law, the aging of batteries is usually simulated by only considering degradation in the initial stages of battery life. However, as the battery ages, the rate of degradation tends to decrease. To account for this, Hoog et al. [61] created a polynomial equation based on the number of cycles, temperature, and the DoD, which models the point where the rate of degradation decreases. The impact of operational temperature was analyzed alongside the impact of the DoD. This equation calculates the relative capacity degradation (RCD) percentage of a battery. This polynomial model differs from other exponential models, as it considers the increasing rate of degradation during the later stages of battery life due to lithium plating. Even though the exact numerical values did not perfectly align with the measured values, the rate of capacity degradation closely corresponded to the measured degradation rate, with error values below 5%.

Omar et al. [75] proposed a new and intricate method for assessing the aging parameters of lithium batteries. The degradation of the batteries was modeled separately based on various factors such as charge–discharge current rates, operating temperatures, and discharge depths. Since a separate equation was created for each stress factor, a total of four equations were presented in the study. These equations were then integrated into MATLAB Simulink to create a general cycle life model under the suggested operating conditions. The researchers argued against the application of the Arrhenius law, as the battery exhibited non-linear behavior throughout its cycle life. They instead used an empirical model with a 3rd-degree polynomial equation to explain the temperature and cycle life development. Additionally, the life cycle development for other factors (Charge–discharge rate and the DoD) is defined as an exponential function. According to the validation test, there is a maximum 5.4% error between the simulated and experimental results.

The models used in electric vehicle batteries discussed above are summarized in Table 5, highlighting their key elements. These different models vary in the stressors they consider, such as cycle time, temperature, the SoC, and C-rate in the outcomes of the aging type they examine. It should be noted that empirical and semi-empirical methods measure a battery's available capacity under reference conditions throughout its lifespan, eliminating variations in available capacity caused by different operating conditions.

Table 5. Overview of semi-empirical/empirical cycling aging model equations reported in the literature.

Source	Model Cases	Type of Result (%)	Model Equation	Model Parameters	Model Error
Hoog et al. [61]	EM	Capacity loss	$\sum_{i=0,j=0}^{n,m} a_i x^i + b_i y^i$	DoD and EFC	RMSE 5
Wang et al. [92]	SEM	Capacity loss	$B \times \exp\left(\frac{-E_a+370.3+C_{rate}}{RT}\right) \times Ah^{0.55}$	Temperature, C-rate, and Ah-throughput	-
Wang et al. [39]	EM	Capacity loss	$(aT^2 + bT + c) \times \exp[(dT + e) \times I_{rate}] \times Ah$	Temperature, C-rate, and Ah-throughput	5%
Sarasketa-Zabala et al. [100]	SEM	Capacity loss	$(\mathbf{i})(a_1 \times DoD^2 + a_2 \times DoD + a_3) \times kAh^{0.87}$ $(\mathbf{ii})(b_3 \times \exp(c_3 DoD) + b_4 \times \exp(c_4 DoD)) \times kAh^{0.65}$	DoD and Ah-throughput	RMSE 1.75
Cordoba-Arenas et al. [90]	SEM	Capacity loss	$\left(a_c + b_c(Ratio)^{d_c} + c_c \times (SoC_{min} - 0.25)^{e_c}\right) \times e^{\frac{-Ea}{RT}} \times Ah^z$	Temperature, DoD, SoC, and Ah-throughput	0.0047%

Table 5. *Cont.*

Source	Model Cases	Type of Result (%)	Model Equation	Model Parameters	Model Error
Saxena et al. [91]	SEM	Remaining capacity	$\left(a_1 \times SoC_{min} \times \left(1 + a_2\Delta SoC + a_3\Delta SoC^2\right) \times \left(\frac{EFC}{100}\right)^{0.453}\right.$	SoC, ΔSoC, and EFC	-
Naumann et al. [99]	SEM	Remaining capacity	$\left(a_{Qloss} \times C - rate + b_{Qloss}\right) \times \left(c_{Qloss}(DoC - 0.6)^3 + d_{Qloss}\right) \times EFC^{z*Qloss}$	Current rate, DoC, and EFC	0.98%
Todeschini et al. [89]	EM	Remaining capacity	$\left(a + b \times \Delta SoC + c \times e^{C-rate}\right) \times n^{1.36}$	ΔSoC, C-rate, and cycle number	0.24%
Petit et al. [103]	SEM	Remaining capacity	$\frac{\lvert I\rvert}{3600} zB(I) \times \exp\frac{-E_a + \alpha\lvert I\rvert}{RT} \times \left(\frac{Q_{loss}}{B(I)\exp\frac{-E_a+\alpha\lvert I\rvert}{RT}}\right)^{1-\frac{1}{z}}$	Current, Temperature, and Ah-throughput	5%
Omar et al. [75]	SEM	Remaining capacity	$(a)\ CL(T) = a \times T^3 - b \times T^2 + c \times T + d (b)\ CL(I_d) = e \times e^{(fI_d)} + g \times e^{(hI_d)} (c)\ CL(I_{ch}) = m \times e^{(nI_{ch})} + o \times e^{(pI_{ch})} (d)\ CL(DoD) = i \times e^{(jDoD)} + k \times e^{(lDoD)}$	Temperature, C-rate, and DoD	5.4%

4. Conclusions

Adaptation of EVs could be achieved by enhancing the feasibility of batteries where lifetime is an essential contributor. The literature documents that the lifespan of batteries decreases over time, which affects the mileage in the lifetime of operation, which could be accelerated under certain usage conditions. This reduction in battery life is primarily caused by complex and multiple side reactions. The occurrence of side reactions is influenced by various factors such as battery manufacturing, battery design, drive cycles, and environmental conditions. This study delves into the behavior and empirical modeling of Li-ion aging, emphasizing the impact and interdependence of various operational stress factors. It also evaluates the degradation mechanisms of batteries and the reactions that contribute to these mechanisms. This study concludes that it is challenging to generalize aging behavior under operational conditions since many stress factors contribute to battery aging, rather than a single factor. Therefore, when creating empirical and semi-empirical aging models for batteries, it is essential to consider the relationships between stress factors and the limitations of the models. The literature shows that there is no perfect aging prediction model but should be decided based on application and relative variables and estimation algorithms should be based on the target application. Key findings of this study are summarized below:

- This study examined various aging models for lithium-ion (Li-ion) batteries used in EVs, focusing on both calendar and cycling aging mechanisms. The findings revealed that model prediction errors were generally lower for calendar aging models compared to cycling aging models, with the literature demonstrating relatively high prediction accuracy for calendar aging.
- Temperature and the SoC are the most critical factors that affect aging mechanisms in batteries. Increased chemical activity caused by high temperatures and degradation mechanisms such as lithium loss accelerate battery degradation. Also, battery performance can be negatively impacted by low temperatures, which increase battery aging. Lithium plating is the main degradation mechanism at low temperatures, unlike high temperatures. Although there is no linear relation between the SoC and battery capacity, the battery capacity tends to decrease more quickly at high SoC values.
- One of the most critical aging mechanisms for cycling and calendar aging is SEI growth. During idle conditions, there is a strong correlation between the SEI layer growth and the negative electrode potential, with a higher SoC leading to increased growth. However, other kinetic effects during cycling can accelerate aging at low SoC. Aging

induced by SoC can take various forms, such as exponential or linear, depending on the operating conditions.

- Another stress factor that occurs during cycling aging is the charge and discharge rate to which the battery is exposed. High rates of charge or discharge can lead to the development of SEI and degradation in the positive electrode. Additionally, it was observed that there exists a strong relationship between the C-rate and temperature: as the temperature rises, the impact of the C ratio decreases. In other words, as the temperature increases, the adverse effects of the C ratio are less reflected in aging. Some models fail to consider this aspect, which can be attributed to the fact that testing is often conducted under accelerated conditions.
- The Arrhenius model is useful for understanding how temperature affects calendar aging. However, it is important to consider that different aging processes occur at temperatures above and below room temperature during cycling. The pre-exponential factor is not a constant value but varies depending on the reaction being studied and the temperature at which it occurs. The pre-exponential factor A shares the same units as the rate constant and argues that a small increase in reaction temperature will produce a significant increase in the magnitude of the reaction rate constant. Therefore, these differences must be taken into account when creating models for cyclic aging below or above room temperature.
- Generally, cycling aging models represent battery cycling using Ah-throughput or the total EFC count. The aging behavior, which is primarily affected by the passivation properties of the SEI layer, is most commonly modeled using a t^z or Ah^z relationship, where $0.5 \leq z \leq 1$.
- Past studies examined the effect of stress factors like temperature, the SoC, and C-rate on different Li-ion chemistries, including LFP, NMC, NCA, LMO, LCO, LTO, and LMO + NMC. Of these, Li-ion chemistries such as LTO and LFP cell chemistries exhibit greater durability against battery degradation compared to other chemistries, making them more suitable for EV applications where longevity is crucial.

To mitigate both calendar and cycling aging, battery management systems (BMSs) in EVs incorporate strategies like temperature regulation, SoC balancing, and smart charging algorithms. Studies suggest that strict control over battery temperature and charge levels, particularly in storage conditions, can significantly extend battery life. The insights from this article offer valuable information to researchers and modelers aiming to improve aging models and develop more effective battery management strategies for EV applications.

Due to variations in voltage and internal resistance between cells, package-level analysis may lead to inaccurate conclusions, necessitating cell-level testing for reliable results. While insights gained from cell-level studies can inform package-level analysis, deriving conclusions about individual cells from package-level data is unreliable due to system noise. As a result, many studies in the literature focus on cell-level analysis for more precise and feasible outcomes.

In conclusion, while substantial progress has been made in understanding the aging mechanisms of Li-ion batteries, particularly in EV contexts, further refinement of aging tests and models is needed. The complex interplay of temperature, the SoC, and C-rate stressors requires more nuanced modeling approaches to optimize battery performance and extend battery life. This review provides a foundation for future research and model improvements, offering a pathway towards more reliable, long-lasting EV batteries.

Author Contributions: Conceptualization, G.Y. and E.C.; formal analysis, G.Y.; investigation, G.Y.; resources, G.Y.; data curation, G.Y.; writing—original draft preparation, G.Y.; writing—review and editing, G.Y. and E.C.; visualization, G.Y. and E.C; supervision, E.C.; project administration, E.C.; funding acquisition, E.C. All authors have read and agreed to the published version of the manuscript.

Funding: This research was funded by Innovation and Networks Executive Agency (INEA) European Union's Horizon 2020 grant number 963646 and the APC was funded by Innovation and Networks Executive Agency (INEA) European Union's Horizon 2020.

Data Availability Statement: The data that supported the findings of this study are available from the corresponding author upon reasonable request.

Acknowledgments: This work was fulfilled within the framework of the HELIOS project, which has received funding from the European Union's Horizon 2020 research and innovation programme under grant agreement No. 963646.

Conflicts of Interest: The authors declare no conflict of interest.

Nomenclature

Abbreviation/Acronym	Definition
A	Exponential Factor
Ah	Ampere-Hour
a-k	Fitting Parameter
C	Current
C-Rate	Current Rate
CD	Charge-Depleting
CEI	Positive electrode Electrolyte Interphase
CL	Conductivity Loss
CS	Charge-Sustaining
CV	Constant Voltage
DC	Direct Current
DoC	Depth of Cycle
DoD	Depth-Of-Discharge
E_a	Activation Energy
ECM	Equivalent Circuit Model
EFC	Equivalent Full Cycles
EV	Electric Vehicle
HEV	Hybrid Electric Vehicle
LAM	Active Material Loss
LCO	Lithium Cobalt Oxide
LFP	Lithium Iron Phosphate
Li-ion	Lithium-Ion
LLI	Loss of Lithium Inventory
LMO	Lithium-Ion Manganese Oxide
LSEV	Low-Speed Electric Vehicles
LTO	Lithium Titanate Oxide
MAE	Mean Absolute Error
N	Number of Cycles
NCA	Nickel Cobalt Aluminum Oxide
NiMH	Nickel Metal Hydride
NMC	Nickel Manganese Cobalt
Q	Total Capacity
Q_{loss}	Capacity Loss
Q_L	Irreversible Capacity Loss
Q_{sd}	Reversible Capacity Loss
Pb-acid	Lead-Acid
R	Gas Constant
RMSE	Root Mean Square Error
SEI	Solid Electrolyte Interphase
SEM	Semi-Empirical Model
SoC	Stage of Charge
T	Temperature
t	Time
USABC	United States Advanced Battery Consortium
V	Voltage
z	Power Law Exponent

References

1. Han, X.; Lu, L.; Zheng, Y.; Feng, X.; Li, Z.; Li, J.; Ouyang, M. A review on the key issues of the lithium ion battery degradation among the whole life cycle. *eTransportation* **2019**, *1*, 100005. [CrossRef]
2. Xiong, R.; Li, L.; Tian, J. Towards a smarter battery management system: A critical review on battery state of health monitoring methods. *J. Power Sources* **2018**, *405*, 18–29. [CrossRef]
3. Sun, X.; Li, Z.; Wang, X.; Li, C. Technology Development of Electric Vehicles: A Review. *Energies* **2019**, *13*, 90. [CrossRef]
4. Kumar, R.R.; Alok, K. Adoption of electric vehicle: A literature review and prospects for sustainability. *J. Clean. Prod.* **2020**, *253*, 119911. [CrossRef]
5. Global EV Outlook 2021—Analysis—IEA. Available online: https://www.iea.org/reports/global-ev-outlook-2021 (accessed on 19 October 2023).
6. Sehil, K.; Alamri, B.; Alqarni, M.; Sallama, A.; Darwish, M. Empirical analysis of high voltage battery pack cells for electric racing vehicles. *Energies* **2021**, *14*, 1556. [CrossRef]
7. Zhang, C.; Li, K.; Mcloone, S.; Yang, Z. Battery modelling methods for electric vehicles—A review. In Proceedings of the 2014 European Control Conference (ECC), Strasbourg, France, 24–27 June 2014; pp. 2673–2678.
8. Hannan, M.A.; Hoque, M.D.M.; Hussain, A.; Yusof, Y.; Ker, A.P.J. State-of-the-Art and Energy Management System of Lithium-Ion Batteries in Electric Vehicle Applications: Issues and Recommendations. *IEEE Access Spec. Sect. Adv. Energy Storage Technol. Appl.* **2018**, *6*, 19362–19378. [CrossRef]
9. Chen, W.; Liang, J.; Yang, Z.; Li, G. A Review of Lithium-Ion Battery for Electric Vehicle Applications and Beyond. *Energy Procedia* **2019**, *158*, 4363–4368. [CrossRef]
10. Stan, A.-I.; Swierczynski, M.; Stroe, D.-I.; Teodorescu, R.; Andreasen, S.J. Lithium ion battery chemistries from renewable energy storage to automotive and back-up power applications—An overview. In Proceedings of the 2014 International Conference on Optimization of Electrical and Electronic Equipment (OPTIM), Bran, Romania, 22–24 May 2014; pp. 713–720. [CrossRef]
11. Chen, X.; Shen, W.; Vo, T.T.; Cao, Z.; Kapoor, A. An overview of lithium-ion batteries for electric vehicles. In Proceedings of the 10th International Power & Energy Conference (IPEC), Ho Chi Minh City, Vietnam, 12–14 December 2012; pp. 230–235. [CrossRef]
12. Lyu, Y.; Wu, X.; Wang, K.; Feng, Z.; Cheng, T.; Liu, Y.; Wang, M.; Chen, R.; Xu, L.; Zhou, J.; et al. An Overview on the Advances of $LiCoO_2$ Positive electrodes for Lithium-Ion Batteries. *Adv. Energy Mater.* **2021**, *11*, 202000982. [CrossRef]
13. Xiong, R.; Pan, Y.; Shen, W.; Li, H.; Sun, F. Lithium-ion battery aging mechanisms and diagnosis method for automotive applications: Recent advances and perspectives. *Renew. Sustain. Energy Rev.* **2020**, *131*, 110048. [CrossRef]
14. Waldmann, T.; Wilka, M.; Kasper, M.; Fleischhammer, M.; Wohlfahrt-Mehrens, M. Temperature dependent ageing mechanisms in Lithium-ion batteries—A Post-Mortem study. *J. Power Sources* **2014**, *262*, 129–135. [CrossRef]
15. Guha, A.; Patra, A. State of Health Estimation of Lithium-Ion Batteries Using Capacity Fade and Internal Resistance Growth Models. *IEEE Trans. Transp. Electrification* **2017**, *4*, 135–146. [CrossRef]
16. Han, X.; Ouyang, M.; Lu, L.; Li, J.; Zheng, Y.; Li, Z. A comparative study of commercial lithium ion battery cycle life in electrical vehicle: Aging mechanism identification. *J. Power Sources* **2014**, *251*, 38–54. [CrossRef]
17. Jaguemont, J.; Boulon, L.; Venet, P.; Dube, Y.; Sari, A. Lithium-Ion Battery Aging Experiments at Subzero Temperatures and Model Development for Capacity Fade Estimation. *IEEE Trans. Veh. Technol.* **2016**, *65*, 4328–4343. [CrossRef]
18. Barré, A.; Deguilhem, B.; Grolleau, S.; Gérard, M.; Suard, F.; Riu, D. A review on lithium-ion battery ageing mechanisms and estimations for automotive applications A review on lithium-ion battery ageing mechanisms and estimations for automotive applications A review on Lithium-ion batteries ageing mechanisms and estimations for automotive applications. *J. Power Sources* **2013**, *241*, 680–689. [CrossRef]
19. Palacín, M.R. Understanding ageing in Li-ion batteries: A chemical issue. *Chem. Soc. Rev.* **2018**, *47*, 4924–4933. [CrossRef]
20. Manzetti, S.; Mariasiu, F. Electric vehicle battery technologies: From present state to future systems. *Renew. Sustain. Energy Rev.* **2015**, *51*, 1004–1012. [CrossRef]
21. Li, D.; Danilov, D.L.; Gao, L.; Yang, Y.; Notten, P.H. Degradation Mechanisms of C6/LiFePO4 Batteries: Experimental Analyses of Cycling-induced Aging. *Electrochim. Acta* **2016**, *210*, 445–455. [CrossRef]
22. Li, D.; Danilov, D.L.; Xie, J.; Raijmakers, L.; Gao, L.; Yang, Y.; Notten, P.H. Degradation Mechanisms of C6/LiFePO4 Batteries: Experimental Analyses of Calendar Aging. *Electrochim. Acta* **2016**, *190*, 1124–1133. [CrossRef]
23. Safari, M.; Delacourt, C. Aging of a Commercial Graphite/LiFePO4 Cell. *J. Electrochem. Soc.* **2011**, *158*, A1123–A1135. [CrossRef]
24. Christensen, J.; Newman, J. A mathematical model for the lithium-ion negative electrode solid electrolyte interphase. *J. Electrochem. Soc.* **2004**, *151*, A1977. [CrossRef]
25. Peled, E.; Menkin, S. Review—SEI: Past, Present and Future. *J. Electrochem. Soc.* **2017**, *164*, A1703–A1719. [CrossRef]
26. Liu, Q.; Du, C.; Shen, B.; Zuo, P.; Cheng, X.; Ma, Y.; Yin, G.; Gao, Y. Understanding undesirable negative electrode lithium plating issues in lithium-ion batteries. *RSC Adv.* **2016**, *6*, 88683–88700. [CrossRef]
27. Birkl, C.R.; Roberts, M.R.; McTurk, E.; Bruce, P.G.; Howey, D.A. Degradation diagnostics for lithium ion cells. *J. Power Sources* **2017**, *341*, 373–386. [CrossRef]
28. Ecker, M.; Gerschler, J.B.; Vogel, J.; Käbitz, S.; Hust, F.; Dechent, P.; Sauer, D.U. Development of a lifetime prediction model for lithium-ion batteries based on extended accelerated aging test data. *J. Power Sources* **2012**, *215*, 248–257. [CrossRef]
29. Hentunen, A.; Lehmuspelto, T.; Suomela, J. Time-domain parameter extraction method for thévenin-equivalent circuit battery models. *IEEE Trans. Energy Convers.* **2014**, *29*, 558–566. [CrossRef]

30. Groot, J.; Hogskola, C.T. Division of Electric Power Engineering, State-of-Health Estimation of Li-ion Batteries: Ageing Models. 2014. Available online: https://research.chalmers.se/en/publication/205605 (accessed on 19 December 2022).
31. Vetter, J.; Novák, P.; Wagner, M.R.; Veit, C.; Möller, K.-C.; Besenhard, J.O.; Winter, M.; Wohlfahrt-Mehrens, M.; Vogler, C.; Hammouche, A. Ageing mechanisms in lithium-ion batteries. *J. Power Sources* **2005**, *147*, 269–281. [CrossRef]
32. Olabi, A.; Maghrabie, H.M.; Adhari, O.H.K.; Sayed, E.T.; Yousef, B.A.; Salameh, T.; Kamil, M.; Abdelkareem, M.A. Battery thermal management systems: Recent progress and challenges. *Int. J. Thermofluids* **2022**, *15*, 100171. [CrossRef]
33. Doyle, M.; Newman, J. The use of mathematical modeling in the design of lithium/polymer battery systems. *Electrochim. Acta* **1995**, *40*, 2191–2196. [CrossRef]
34. Newman, J.; Tiedemann, W. Potential and Current Distribution in Electrochemical Cells: Interpretation of the Half-Cell Voltage Measurements as a Function of Reference-Electrode Location. *J. Electrochem. Soc.* **1993**, *140*, 1961–1968. [CrossRef]
35. Millner, A. Modeling Lithium Ion battery degradation in electric vehicles. In Proceedings of the 2010 IEEE Conference on Innovative Technologies for an Efficient and Reliable Electricity Supply, Waltham, MA, USA, 27–29 September 2010; pp. 349–356.
36. Lehtola, T.A.; Zahedi, A. Electric Vehicle Battery Cell Cycle Aging in Vehicle to Grid Operations: A Review. *IEEE J. Emerg. Sel. Top. Power Electron.* **2019**, *9*, 423–437. [CrossRef]
37. Nájera, J.; Arribas, J.; de Castro, R.; Núñez, C. Semi-empirical ageing model for LFP and NMC Li-ion battery chemistries. *J. Energy Storage* **2023**, *72*, 108016. [CrossRef]
38. Werner, D.; Paarmann, S.; Wetzel, T. Calendar Aging of Li-Ion Cells—Experimental Investigation and Empirical Correlation. *Batteries* **2021**, *7*, 28. [CrossRef]
39. Wang, J.; Purewal, J.; Liu, P.; Hicks-Garner, J.; Soukazian, S.; Sherman, E.; Sorenson, A.; Vu, L.; Tataria, H.; Verbrugge, M.W. Degradation of lithium ion batteries employing graphite negatives and nickel–cobalt–manganese oxide + spinel manganese oxide positives: Part 1, aging mechanisms and life estimation. *J. Power Sources* **2014**, *269*, 937–948. [CrossRef]
40. Pan, W.; Chen, Q.; Zhu, M.; Tang, J.; Wang, J. A data-driven fuzzy information granulation approach for battery state of health forecasting. *J. Power Sources* **2020**, *475*, 228716. [CrossRef]
41. Severson, K.A.; Attia, P.M.; Jin, N.; Perkins, N.; Jiang, B.; Yang, Z.; Chen, M.H.; Aykol, M.; Herring, P.K.; Fraggedakis, D.; et al. Data-driven prediction of battery cycle life before capacity degradation. *Nat. Energy* **2019**, *4*, 383–391. [CrossRef]
42. Goud, J.S.; Kalana, R.; Singh, B. An Online Method of Estimating State of Health of a Li-Ion Battery. *IEEE Trans. Energy Convers.* **2020**, *36*, 111–119. [CrossRef]
43. Li, Y.; Liu, K.; Foley, A.M.; Zülke, A.; Berecibar, M.; Nanini-Maury, E.; Van Mierlo, J.; Hoster, H.E. Data-driven health estimation and lifetime prediction of lithium-ion batteries: A review. *Renew. Sustain. Energy Rev.* **2019**, *113*, 109254. [CrossRef]
44. Ng, M.-F.; Zhao, J.; Yan, Q.; Conduit, G.J.; Seh, Z.W. Predicting the state of charge and health of batteries using data-driven machine learning. *Nat. Mach. Intell.* **2020**, *2*, 161–170. [CrossRef]
45. Gasper, P.; Gering, K.; Dufek, E.; Smith, K. Challenging Practices of Algebraic Battery Life Models through Statistical Validation and Model Identification via Machine-Learning. *J. Electrochem. Soc.* **2021**, *168*, 020502. [CrossRef]
46. Krupp, A.; Beckmann, R.; Diekmann, T.; Ferg, E.; Schuldt, F.; Agert, C. Calendar aging model for lithium-ion batteries considering the influence of cell characterization. *J. Energy Storage* **2021**, *45*, 103506. [CrossRef]
47. Eddahech, A.; Briat, O.; Vinassa, J.-M. Performance comparison of four lithium–ion battery technologies under calendar aging. *Energy* **2015**, *84*, 542–550. [CrossRef]
48. Stiaszny, B.; Ziegler, J.C.; Krauß, E.E.; Zhang, M.; Schmidt, J.P.; Ivers-Tiffée, E. Electrochemical characterization and post-mortem analysis of aged LiMn2O4–NMC/graphite lithium ion batteries part II: Calendar aging. *J. Power Sources* **2014**, *258*, 61–75. [CrossRef]
49. McBrayer, J.D.; Rodrigues, M.-T.F.; Schulze, M.C.; Abraham, D.P.; Apblett, C.A.; Bloom, I.; Carroll, G.M.; Colclasure, A.M.; Fang, C.; Harrison, K.L.; et al. Calendar aging of silicon-containing batteries. *Nat. Energy* **2021**, *6*, 866–872. [CrossRef]
50. Lammer, M.; Königseder, A.; Gluschitz, P.; Hacker, V. Influence of aging on the heat and gas emissions from commercial lithium ion cells in case of thermal failure. *J. Electrochem. Sci. Eng.* **2018**, *8*, 101–110. [CrossRef]
51. Deichmann, E.J.; Torres-Castro, L.; Lamb, J.H.; Karulkar, M.P.; Ivanov, S.; Grosso, C.; Gray, L.S.; Langendorf, J.L.; Garzon, F. Investigating the Effects of Lithium Deposition on the Abuse Response of Lithium-Ion Batteries. *J. Electrochem. Soc.* **2020**, *167*, 090552. [CrossRef]
52. Sarasketa-Zabala, E.; Gandiaga, I.; Rodriguez-Martinez, L.; Villarreal, I. Calendar ageing analysis of a LiFePO4/graphite cell with dynamic model validations: Towards realistic lifetime predictions. *J. Power Sources* **2014**, *272*, 45–57. [CrossRef]
53. Omar, N.; Firouz, Y.; Timmermans, J.M.; Monem, M.A.; Gualous, H.; Coosemans, T.; Bossche, P.V.D.; Van Mierlo, J. Lithium iron phosphate—assessment of calendar life and change of battery parameters. In Proceedings of the 2014 IEEE Vehicle Power and Propulsion Conference (VPPC), Coimbra, Portugal, 27–30 October 2014; pp. 1–5.
54. Grolleau, S.; Delaille, A.; Gualous, H.; Gyan, P.; Revel, R.; Bernard, J.; Redondo-Iglesias, E.; Peter, J. Calendar aging of commercial graphite/LiFePO4 cell—Predicting capacity fade under time dependent storage conditions. *J. Power Sources* **2014**, *255*, 450–458. [CrossRef]
55. Kassem, M.; Bernard, J.; Revel, R.; Pélissier, S.; Duclaud, F.; Delacourt, C. Calendar aging of a graphite/LiFePO4 cell. *J. Power Sources* **2012**, *208*, 296–305. [CrossRef]
56. Wildfeuer, L.; Karger, A.; Aygül, D.; Wassiliadis, N.; Jossen, A.; Lienkamp, M. Experimental degradation study of a commercial lithium-ion battery. *J. Power Sources* **2023**, *560*, 232498. [CrossRef]

57. Karger, A.; Schmitt, J.; Kirst, C.; Singer, J.P.; Wildfeuer, L.; Jossen, A. Mechanistic calendar aging model for lithium-ion batteries. *J. Power Sources* **2023**, *578*, 233208. [CrossRef]
58. Jaguemont, J.; Boulon, L.; Venet, P.; Dube, Y.; Sari, A. Low temperature aging tests for lithium-ion batteries. In Proceedings of the 2015 IEEE 24th International Symposium on Industrial Electronics (ISIE), Buzios, Brazil, 3–5 June 2015; pp. 1284–1289.
59. Maures, M.; Zhang, Y.; Martin, C.; Delétage, J.-Y.; Vinassa, J.-M.; Briat, O. Impact of temperature on calendar ageing of Lithium-ion battery using incremental capacity analysis. *Microelectron. Reliab.* **2019**, *100–101*, 113364. [CrossRef]
60. Schmalstieg, J.; Käbitz, S.; Ecker, M.; Sauer, D.U. A holistic aging model for Li(NiMnCo)O_2 based 18650 lithium-ion batteries. *J. Power Sources* **2014**, *257*, 325–334. [CrossRef]
61. De Hoog, J.; Timmermans, J.-M.; Ioan-Stroe, D.; Swierczynski, M.; Jaguemont, J.; Goutam, S.; Omar, N.; Van Mierlo, J.; Van Den Bossche, P. Combined cycling and calendar capacity fade modeling of a Nickel-Manganese-Cobalt Oxide Cell with real-life profile validation. *Appl. Energy* **2017**, *200*, 47–61. [CrossRef]
62. Zheng, Y.; He, Y.-B.; Qian, K.; Li, B.; Wang, X.; Li, J.; Miao, C.; Kang, F. Effects of state of charge on the degradation of LiFePO4/graphite batteries during accelerated storage test. *J. Alloys Compd.* **2015**, *639*, 406–414. [CrossRef]
63. Redondo-Iglesias, E.; Venet, P.; Pelissier, S. Eyring acceleration model for predicting calendar ageing of lithium-ion batteries Eyring acceleration model for predict-ing calendar ageing of lithium-ion batteries Eyring acceleration model for predicting calendar ageing of lithium-ion batteries. *J. Energy Storage* **2017**, *13*, 176–183. [CrossRef]
64. Dai, H.; Zhang, X.; Gu, W.; Wei, X.; Sun, Z. A semi-empirical capacity degradation model of ev li-ion batteries based on eyring equation. In Proceedings of the 2013 IEEE Vehicle Power and Propulsion Conference (VPPC), Beijing, China, 15–18 October 2013; pp. 1–5.
65. Redondo-Iglesias, E.; Venet, P.; Pelissier, S. Influence of the non-conservation of SoC value during calendar ageing tests on modelling the capacity loss of batteries. In Proceedings of the 2015 Tenth International Conference on Ecological Vehicles and Renewable Energies (EVER), Monte-Carlo, Monaco, 31 March–2 April 2015; pp. 1–5.
66. Su, L.; Zhang, J.; Huang, J.; Ge, H.; Li, Z.; Xie, F.; Liaw, B.Y. Path dependence of lithium ion cells aging under storage conditions. *J. Power Sources* **2016**, *315*, 35–46. [CrossRef]
67. Naumann, M.; Schimpe, M.; Keil, P.; Hesse, H.C.; Jossen, A. Analysis and modeling of calendar aging of a commercial LiFePO4/graphite cell. *J. Energy Storage* **2018**, *17*, 153–169. [CrossRef]
68. Xu, B.; Oudalov, A.; Ulbig, A.; Andersson, G.; Kirschen, D.S. Modeling of lithium-ion battery degradation for cell life assessment. *IEEE Trans. Smart Grid* **2016**, *9*, 1131–1140. [CrossRef]
69. Montaru, M.; Fiette, S.; Koné, J.-L.; Bultel, Y. Calendar ageing model of Li-ion battery combining physics-based and empirical approaches. *J. Energy Storage* **2022**, *51*, 104544. [CrossRef]
70. Dubarry, M.; Truchot, C.; Liaw, B.Y. Synthesize battery degradation modes via a diagnostic and prognostic model. *J. Power Sources* **2012**, *219*, 204–216. [CrossRef]
71. Ma, Z.; Wang, Z.; Xiong, R.; Jiang, J. A mechanism identification model based state-of-health diagnosis of lithium-ion batteries for energy storage applications. *J. Clean. Prod.* **2018**, *193*, 379–390. [CrossRef]
72. Keil, P.; Schuster, S.F.; Wilhelm, J.; Travi, J.; Hauser, A.; Karl, R.C.; Jossen, A. Calendar Aging of Lithium-Ion Batteries. *J. Electrochem. Soc.* **2016**, *163*, A1872–A1880. [CrossRef]
73. Geisbauer, C.; Wöhrl, K.; Koch, D.; Wilhelm, G.; Schneider, G.; Schweiger, H.-G. Comparative study on the calendar aging behavior of six different lithium-ion cell chemistries in terms of parameter variation. *Energies* **2021**, *14*, 3358. [CrossRef]
74. Schuster, S.F.; Bach, T.; Fleder, E.; Müller, J.; Brand, M.; Sextl, G.; Jossen, A. Nonlinear aging characteristics of lithium-ion cells under different operational conditions. *J. Energy Storage* **2015**, *1*, 44–53. [CrossRef]
75. Omar, N.; Monem, M.A.; Firouz, Y.; Salminen, J.; Smekens, J.; Hegazy, O.; Gaulous, H.; Mulder, G.; Van Den Bossche, P.; Coosemans, T.; et al. Lithium iron phosphate based battery—Assessment of the aging parameters and development of cycle life model. *Appl. Energy* **2014**, *113*, 1575–1585. [CrossRef]
76. Jaguemont, J.; Boulon, L.; Dubé, Y. A comprehensive review of lithium-ion batteries used in hybrid and electric vehicles at cold temperatures. *Appl. Energy* **2016**, *164*, 99–114. [CrossRef]
77. Zheng, Y.; Ouyang, M.; Lu, L.; Li, J. Understanding aging mechanisms in lithium-ion battery packs: From cell capacity loss to pack capacity evolution. *J. Power Sources* **2015**, *278*, 287–295. [CrossRef]
78. Schimpe, M.; von Kuepach, M.E.; Naumann, M.; Hesse, H.C.; Smith, K.; Jossen, A. Comprehensive Modeling of Temperature-Dependent Degradation Mechanisms in Lithium Iron Phosphate Batteries. *J. Electrochem. Soc.* **2018**, *165*, A181–A193. [CrossRef]
79. Attia, P.M.; Chueh, W.C.; Harris, S.J. Revisiting the $t^{0.5}$ Dependence of SEI Growth. *J. Electrochem. Soc.* **2020**, *167*, 090535. [CrossRef]
80. Pan, B.; Dong, D.; Wang, J.; Nie, J.; Liu, S.; Cao, Y.; Jiang, Y. Aging mechanism diagnosis of lithium ion battery by open circuit voltage analysis. *Electrochim. Acta* **2020**, *362*, 137101. [CrossRef]
81. Wegmann, R.; Döge, V.; Sauer, D.U. Assessing the potential of a hybrid battery system to reduce battery aging in an electric vehicle by studying the cycle life of a graphite|NCA high energy and a LTO|metal oxide high power battery cell considering realistic test profiles. *Appl. Energy* **2018**, *226*, 197–212. [CrossRef]
82. Zhang, Y.; Wang, C.-Y.; Tang, X. Cycling degradation of an automotive LiFePO4 lithium-ion battery. *J. Power Sources* **2010**, *196*, 1513–1520. [CrossRef]

83. Yang, N.; Zhang, X.; Shang, B.; Li, G. Unbalanced discharging and aging due to temperature differences among the cells in a lithium-ion battery pack with parallel combination. *J. Power Sources* **2016**, *306*, 733–741. [CrossRef]
84. Baghdadi, I.; Briat, O.; Delétage, J.-Y.; Gyan, P.; Vinassa, J.-M. Lithium battery aging model based on Dakin's degradation approach. *J. Power Sources* **2016**, *325*, 273–285. [CrossRef]
85. Dakin, T.W. Electrical Insulation Deterioration Treated as a Chemical Rate Phenomenon. *Trans. Am. Inst. Electr. Eng.* **1948**, *67*, 113–122. [CrossRef]
86. Wu, X.; Wang, W.; Sun, Y.; Wen, T.; Chen, J.; Du, J. Study on the Capacity Fading Effect of Low-Rate Charging on Lithium-Ion Batteries in Low-Temperature Environment. *World Electr. Veh. J.* **2020**, *11*, 55. [CrossRef]
87. Burow, D.; Sergeeva, K.; Calles, S.; Schorb, K.; Börger, A.; Roth, C.; Heitjans, P. Inhomogeneous degradation of graphite negative electrodes in automotive lithium ion batteries under low-temperature pulse cycling conditions. *J. Power Sources* **2016**, *307*, 806–814. [CrossRef]
88. Rauhala, T.; Jalkanen, K.; Romann, T.; Lust, E.; Omar, N.; Kallio, T. Low-temperature aging mechanisms of commercial graphite/LiFePO4 cells cycled with a simulated electric vehicle load profile—A post-mortem study. *J. Energy Storage* **2018**, *20*, 344–356. [CrossRef]
89. Todeschini, F.; Onori, S.; Rizzoni, G. An experimentally validated capacity degradation model for Li-ion batteries in PHEVs applications. *IFAC Proc. Vol.* **2012**, *45*, 456–461. [CrossRef]
90. Cordoba-Arenas, A.; Onori, S.; Guezennec, Y.; Rizzoni, G. Capacity and power fade cycle-life model for plug-in hybrid electric vehicle lithium-ion battery cells containing blended spinel and layered-oxide positive electrodes. *J. Power Sources* **2015**, *278*, 473–483. [CrossRef]
91. Saxena, S.; Hendricks, C.; Pecht, M. Cycle life testing and modeling of graphite/LiCoO2 cells under different state of charge ranges. *J. Power Sources* **2016**, *327*, 394–400. [CrossRef]
92. Wang, J.; Liu, P.; Hicks-Garner, J.; Sherman, E.; Soukiazian, S.; Verbrugge, M.; Tataria, H.; Musser, J.; Finamore, P. Cycle-life model for graphite-LiFePO4 cells. *J. Power Sources* **2010**, *196*, 3942–3948. [CrossRef]
93. Bloom, I.; Cole, B.; Sohn, J.; Jones, S.; Polzin, E.; Battaglia, V.; Henriksen, G.; Motloch, C.; Richardson, R.; Unkelhaeuser, T.; et al. An accelerated calendar and cycle life study of Li-ion cells. *J. Power Sources* **2001**, *101*, 238–247. [CrossRef]
94. Gao, Y.; Jiang, J.; Zhang, C.; Zhang, W.; Jiang, Y. Aging mechanisms under different state-of-charge ranges and the multi-indicators system of state-of-health for lithium-ion battery with Li(NiMnCo)O_2 positive electrode. *J. Power Sources* **2018**, *400*, 641–651. [CrossRef]
95. Gantenbein, S.; Schönleber, M.; Weiss, M.; Ivers-Tiffée, E. Capacity Fade in Lithium-Ion Batteries and Cyclic Aging over Various State-of-Charge Ranges. *Sustainability* **2019**, *11*, 6697. [CrossRef]
96. Wikner, E.; Thiringer, T. Extending Battery Lifetime by Avoiding High SOC. *Appl. Sci.* **2018**, *8*, 1825. [CrossRef]
97. Benavente-Araoz, F.; Varini, M.; Lundblad, A.; Cabrera, S.; Lindbergh, G. Effect of Partial Cycling of NCA/Graphite Cylindrical Cells in Different SOC Intervals. *J. Electrochem. Soc.* **2020**, *167*, 040529. [CrossRef]
98. Preger, Y.; Barkholtz, H.M.; Fresquez, A.; Campbell, D.L.; Juba, B.W.; Romàn-Kustas, J.; Ferreira, S.R.; Chalamala, B.R. Degradation of Commercial Lithium-Ion Cells as a Function of Chemistry and Cycling Conditions. *J. Electrochem. Soc.* **2020**, *167*, 120532. [CrossRef]
99. Naumann, M.; Spingler, F.B.; Jossen, A. Analysis and modeling of cycle aging of a commercial LiFePO4/graphite cell. *J. Power Sources* **2020**, *451*, 227666. [CrossRef]
100. Sarasketa-Zabala, E.; Gandiaga, I.; Martinez-Laserna, E.; Rodriguez-Martinez, L.; Villarreal, I. Cycle ageing analysis of a LiFePO4/graphite cell with dynamic model validations: Towards realistic lifetime predictions. *J. Power Sources* **2015**, *275*, 573–587. [CrossRef]
101. Groot, J.; Swierczynski, M.; Stan, A.I.; Kær, S.K. On the complex ageing characteristics of high-power LiFePO4/graphite battery cells cycled with high charge and discharge currents. *J. Power Sources* **2015**, *286*, 475–487. [CrossRef]
102. Wu, Y.; Keil, P.; Schuster, S.F.; Jossen, A. Impact of Temperature and Discharge Rate on the Aging of a $LiCoO_2/LiNi_{0.8}Co_{0.15}Al_{0.05}O_2$ Lithium-Ion Pouch Cell. *J. Electrochem. Soc.* **2017**, *164*, A1438–A1445. [CrossRef]
103. Petit, M.; Prada, E.; Sauvant-Moynot, V. Development of an empirical aging model for Li-ion batteries and application to assess the impact of Vehicle-to-Grid strategies on battery lifetime. *Appl. Energy* **2016**, *172*, 398–407. [CrossRef]
104. Barcellona, S.; Piegari, L. Effect of current on cycle aging of lithium ion batteries. *J. Energy Storage* **2020**, *29*, 101310. [CrossRef]
105. Saldana, G.; Martin, J.I.S.; Zamora, I.; Asensio, F.J.; Onederra, O.; Gonzalez, M. Empirical Electrical and Degradation Model for Electric Vehicle Batteries. *IEEE Access* **2020**, *8*, 155576–155589. [CrossRef]
106. Krupp, A.; Beckmann, R.; Diekmann, T.; Liebig, G.; Ferg, E.; Schuldt, F.; Agert, C. Semi-empirical cyclic aging model for stationary storages based on graphite negative electrode aging mechanisms. *J. Power Sources* **2023**, *561*, 232721. [CrossRef]
107. Kucinskis, G.; Bozorgchenani, M.; Feinauer, M.; Kasper, M.; Wohlfahrt-Mehrens, M.; Waldmann, T. Arrhenius plots for Li-ion battery ageing as a function of temperature, C-rate, and ageing state—An experimental study. *J. Power Sources* **2022**, *549*, 232129. [CrossRef]
108. Karger, A.; Schmitt, J.; Kirst, C.; Singer, J.P.; Wildfeuer, L.; Jossen, A. Mechanistic cycle aging model for the open-circuit voltage curve of lithium-ion batteries. *J. Power Sources* **2023**, *593*, 233947. [CrossRef]
109. Cordoba-Arenas, A.; Onori, S.; Rizzoni, G.; Fan, G. Aging Propagation in Advanced Battery Systems: Preliminary Results. *IFAC Proc. Vol.* **2013**, *46*, 313–318. [CrossRef]

110. Jalkanen, K.; Karppinen, J.; Skogström, L.; Laurila, T.; Nisula, M.; Vuorilehto, K. Cycle aging of commercial NMC/graphite pouch cells at different temperatures. *Appl. Energy* **2015**, *154*, 160–172. [CrossRef]
111. Käbitz, S.; Gerschler, J.B.; Ecker, M.; Yurdagel, Y.; Emmermacher, B.; André, D.; Mitsch, T.; Sauer, D.U. Cycle and calendar life study of a graphite | LiNi1/3Mn1/3Co1/3O2 Li-ion high energy system. Part A: Full cell characterization. *J. Power Sources* **2013**, *239*, 572–583. [CrossRef]